의학박사 학위논문

관상동맥 전산화단층촬영을 이용한 동맥경화반 부피의 자동 측정에서 위치 적응 분할 방법의 개념증명 연구

2016년 8월

서울대학교 대학원

의학과 영상의학 전공

신 청 일

Thesis for the Degree of Doctor of Philosophy in Medicine

Location–adaptive Threshold Segmentation for Automated Quantification of Coronary Atherosclerotic Plaque Volume Using Coronary Computed Tomographic Angiography: A Proof of Concept

August 2016

Graduate School of Medicine

Seoul National University

Radiology Major

Cheong-Il Shin

Abstract

Background: Automated methods that use noninvasive coronary computed tomographic angiography (CCTA) have been tried in coronary artery plaque measurement instead of labor-intensive manual methods or invasive intravascular ultrasound (IVUS). These automated methods have shown promising results, but has also shown lower interplatform reproducibility.

Purpose: This study: 1) investigates interplatform reproducibility in automated plaque quantification programs, 2) proves that luminal attenuation differ in lumen size using a phantom, 3) develops an automated segmentation algorithm of outer vessel boundary, and 4) devises and validates a new concept of inner lumen segmentation.

Materials and Methods: The first part of this four-part study was to automatically measure total plaque volume (TPV) and lumen volume (LV) using three commercially available software programs. Agreement was evaluated for each pair of seventeen coronary artery target segments, with the reference standard of IVUS. Plastic phantom simulating vessels of different diameters immersed in contrast mixtures were scanned for a phantom study that used computed tomography; in addition, intraluminal attenuations were measured. Dedicated software for automated segmentation of the outer vessel boundary was developed in the following order: 1) initial crude tubular segment creation using a region-growing method, 2) initial centerline extraction using a minimum cost path, 3) curved planar reformation and perpendicular plane generation, 4) outer boundary determination and tuning using leakage interpolation, rolling ball curve fitting, and convex hull

algorithm, and 5) final centerline determination at the center of the gravity in the outer boundary. A new concept of lumen segmentation, a location-adaptive threshold method was devised, in which a lower attenuation value was applied in stenotic locations within a target segment for edge detection between the lumen and vessel wall, versus a scan-adaptive threshold method in which a certain single threshold value was applied through target segment according to the enhancement degree in a CCTA scan. To validate this concept, LV and TPV of 22 coronary artery segments from 15 patients were calculated in different ways to apply threshold levels at each cross-section according to the definitions used in the scan-adaptive and location-adaptive threshold methods. These were then compared to IVUS-derived parameters as a reference standard. In addition, subgroup analysis according to lumen size was also performed per cross-section in segments with noncalcified plaques.

Results: Intraclass correlation coefficients (ICC) for TPV and LV automatically measured by commercially available software programs were 0.369 to 0.482 and 0.759, respectively. The phantom study demonstrated that intraluminal attenuation of simulated vessels decreased with a decrease in diameter. A newly developed software for outer vessel segmentation showed excellent agreement with IVUS in vessel volume quantification (ICC, 0.919). In the validation study for a new concept, the mean value of LV (mean ± standard error, 93.0 ± 11.2 mm^3 vs 93.7 ± 10.0 mm^3) and TPV (114.4 ± 11.4 mm^3 vs 125.7 ± 15.5 mm^3) between IVUS and the location-adaptive threshold method was not significantly different ($P = 0.999$). Scan-adaptive threshold methods significantly underestimated and overestimated the mean value of LV (78.4 ± 10.2 mm^3) and TPV (141.1 ± 16.4 mm^3), respectively ($P < 0.05$).

Agreement of LV with the reference standard was better for the location-adaptive threshold method (ICC, 0.930) than for the scan-adaptive method (ICC, 0.872). Subgroup analysis revealed a difference in the mean value of the lumen area between the scan-adaptive and location-adaptive threshold methods was significant in the smaller lumen group (3.85 mm^2 vs 4.92 mm^2, $P<0.001$), but not significant in the larger lumen group (7.09 mm^2 vs 7.01 mm^2, $P=0.336$).

Conclusion: Based on the results of a phantom study that showed that intraluminal attenuation decreases with diminution of vessel diameters, the proposed location-adaptive threshold method, a novel concept for lumen segmentation, was shown to be more accurate than the scan-adaptive threshold method.

Keywords: Location-adaptive threshold method, scan-adaptive threshold method, atherosclerotic plaque, coronary computed tomographic angiography, automated plaque quantification, full width at half maximum, intravascular ultrasound

Student Number: 2008-31012

Table of Contents

List of Tables

List of Figures

List of Abbreviations

ANOVA = Analysis of Variance

CCTA = Coronary Computed Tomographic Angiography

CI = Confidence Interval

CPR = Curved Planar Reformation

CT = Computed Tomography

FWHM = Full Width at Half Maximum

HU = Hounsfield Unit

ICC = Intraclass Correlation Coefficient

IVUS = Intravascular Ultrasound

LA = Lumen Area

LV = Lumen Volume

OCT = Optical Coherence Tomography

TPV = Total Plaque Volume

Introduction

Intensive lipid-lowering therapy may reduce coronary artery plaque burden (1,2), which is a strong predictor of cardiovascular events (3-5). As therapies continue to develop and improve, quantification of the coronary plaque burden is important to select indications of medical intervention and evaluate treatment response. Intravascular ultrasound (IVUS) is the modality that has been established as the gold standard for in vivo imaging of coronary artery especially the outer vessel wall as well as the inner boundary with high resolution that allows plaque quantification (6,7). However, IVUS is an invasive and expensive method and is not suitable for routine applications related to risk stratification for primary prevention and monitor for therapeutic effect. Therefore, the development of a noninvasive quantification of coronary artery plaque with clinically acceptable accuracy is required.

Recent advances in multi-detector row computed tomography technology providing improved spatial and temporal resolution with wide coverage has allowed coronary computed tomographic angiography (CCTA) to become the premier modality for noninvasive evaluation of coronary arteries. Several studies have shown high diagnostic accuracy for anatomical luminal stenosis using CCTA with 95-99% sensitivity and 64-87% specificity (8,9).

CCTA can provide extraluminal information of coronary noncalcified plaques as well as calcified plaques in addition to the assessment of contrast-enhanced luminal lesion. Several studies have been published in the last decade that compared CCTA with IVUS and demonstrated excellent

correlation for the detection of intracoronary plaque with 79-100% sensitivity and 88-99% specificity (10). The possibility of discrimination of noncalcified plaques into fibrous and lipid-rich or necrotic components using CCTA has been recently proposed as classified by IVUS-based imaging for tissue characterization (11,12).

In addition to characterization, coronary plaque quantification has been tried with CCTA in a noninvasive manner. In 2004, Achenbach et al. first reported the ability of MDCT to detect and quantify atherosclerotic plaque in nonstenotic coronary arteries (13). Plaque areas were manually traced on contiguous 1 mm thick cross-sectional images of coronary arteries. Plaque volume were calculated by multiplying area and slice increment with a Pearson's correlation of 0.8 for plaque volumes measured with CCTA and IVUS. Several studies reported that plaque volumes measured by using manually tracing plaques on CCTA have shown a good correlation with IVUS-derived values (14-17); in addition, manual measurements also may be a current reference tool for the quantification of coronary plaque burdens from CCTA (18). However, manually delineating and tracing plaque areas in several contiguous cross-sections of coronary arteries can be time-consuming and subject to relevant inter-observer reliability (15,18-20).

Some attempts have been undertaken to measure the coronary plaque volume in an automated fashion. A variety of commercial software algorithms have been introduced to allow automated quantification of noncalcified coronary artery plaque and prior studies have overcome the shortages of time-consuming and large subjective bias in the manual method (21-25). However, a recent study by Oberoi et al., showed that currently available noncalcified

plaque quantification software provides poor interplatform reproducibility (26). The authors performed an analyses of identical datasets for each patient using three commercially available software platforms (Aquarius, TeraRecon; Circulation, Siemens; Vitrea, Vital Image) to quantify noncalcified coronary artery plaque volume. The Pearson correlation coefficients among the three platforms were 0.550-0.677.

Automatically measured coronary plaque volume using different software programs cannot be totally identical because individual companies use distinct algorithms; however, low interplatform reproducibility hinders automated methods from general applications for coronary plaque volume measurement. Commercially available software usually calculates coronary artery plaque volume as vessel volume minus lumen volume; therefore, low interplatform reproducibility would be due to variations of the vessel volume or lumen volume or both measured from each software program. The effective technological development of automated methods requires knowing which variant affects the low interplatform reproducibility; however, Oberoi et al. did not assess this aspect (26) and it was therefore first investigated with the reference standards based on IVUS parameters.

Three dimensional volume rendering (VR) image or surface shaded display (SSD) sometimes overestimates vascular luminal stenosis in clinical practice. VR or SSD express results according to the input threshold level; therefore, exaggerated stenosis on VR or SSD suggests that intraluminal attenuation decreases in the stenotic portion. Consequently, luminal segmentation based on threshold methods commonly used in currently available automated plaque quantification software programs may need

modification for the application of threshold methods. There has been no published study on the relationship between lumen size and attenuation; therefore, a phantom study was done to confirm that luminal attenuation differ in vessel size as a second purpose of this study.

A third purpose of this study was to devise a new concept of lumen segmentation based on results of the phantom study (named as the location-adaptive threshold method) and as a part of the improvement in plaque volume quantification. It was then assessed to be more effective compared to scan-adaptive threshold methods using clinical data. Before performing this study, a dedicated software for automated segmentation of the outer vessel boundary was developed to provide a more accurate outer boundary segmentation and create a working program for the validation of a location-adaptive threshold method.

The objectives of this thesis, therefore, were the following: 1) to investigate the factors that affect the interplatform reproducibility of automated plaque quantification programs, 2) to prove that luminal attenuation varies in lumen size using a phantom, 3) to develop an automated segmentation algorithm for the outer vessel boundary, and 4) to devise and validate a new concept for inner lumen segmentation.

Materials and Methods

Part I. Clinical cross sectional study: Interplatform reproducibility of automated methods for coronary plaque volume measurement

Patient population

This study included 30 target segments from 25 consecutive patients with suspected or known coronary artery disease who underwent CCTA and clinically indicated invasive coronary angiography with IVUS from March 1, 2009 to June 30, 2010 at Seoul National University Hospital. Exclusion criteria were 1) suboptimal image quality due to motion artifact in the target segment on CCTA (n = 6) and 2) failure of segmentation by any software (n= 7; 2 cases in Xelis, 3 cases in AWS, 1 case in Vitrea, and 1 case in both Xelis and AWS). After excluding thirteen segments, 14 patients (65.2 years; male, 78.6%) and 17 coronary artery segments were included in the final analysis.

CT image acquisition and reconstruction

CCTA was performed in compliance with the guidelines of Society of Cardiovascular Computed Tomography guidelines (27). Oral metoprolol (Betaloc; AstraZeneca, Sweden) was administrated for any patient with a heart rate ≥ 65 beat/min 40-60 min prior to CT examination, unless the subject had a contraindication to beta-blockers. Immediately before image

acquisition, 0.4 mg sublingual nitroglycerin (NitroQuick, Ethex, St. Louis, Mo) was administrated to all patients except contraindicated. An initial 60 mL of nonionic contrast medium (Ultravist 370; Schering, Berlin, Germany) was injected into an antecubital vein at a flow rate of 5 mL/s, followed by an additional 20 mL of a nonionic contrast medium and 50 mL of mixed normal saline (80%) and contrast medium (20%) at a rate of 4 mL/s with use of a dual power injector. CT scan started 8 seconds after a threshold trigger of 150 HU in the mid ascending aorta using the bolus triggering method.

CCTA data were acquired with: 1) a dual-source CT scanner (Somatom Definition, Siemens, Forchheim, Germany), 2) a 16 slice CT scanner (Sensation 16, Siemens, Forchheim, Germany), and 3) a 256 slice CT scanner (iCT, Philips medical Systems, Best, The Netherlands). The scan parameters were: 32 × 0.6 mm/128 × 0.625 mm/16 × 0.75 mm collimation, a tube voltage of 100 kVp or 120 kVp depending on body habitus, tube currents of 104-620 mA depending on body habitus, and rotation times of 270-370 ms. The images were reconstructed with a retrospective electrocardiographic-gated technique with a monosegment reconstruction algorithm. Motion-free data sets, typically in mid-diastole, were collected. Reconstruction parameters included a slice thickness of 0.8-1 mm, increments of 0.5-0.7 mm, and a medium soft convolution kernel. The estimated effected radiation dose for CCTA ranged from 3.0 mSv to 9.4 mSv using the dose-length product with an organ-specific conversion factor k of 0.014 mSv/mGy/cm.

CT image analysis

Analyses of identical datasets for each target segment were

performed with three commercially available software programs: Xelis (Xelis, Version 1.0.4.3; Infinitt Healthcare, Korea), AWS (Advantage Workstation with CardIQ software, Version 2.0; GE Healthcare, Milwaukee, Wisconsin) and Vitrea (Vitrea, Version 2; Vital Images, Plymouth, Minnesota). To avoid bias, the observer completed all measurements on a single workstation before moving to the next workstation, was blinded to patient-identifying information, and evaluated subjects in a random order on each workstation. Attention was paid to ensuring that the length and location of analyzed segments were consistent for all patients across each software program using indicators created by IVUS data. Automated analysis was performed using the manufactures default settings and a manual edition was added if necessary. Both vessel volume and lumen volume were provided in Xelis and AWS software; subsequently, plaque volume was calculated as vessel volume minus lumen volume. Vitrea software was excluded in the lumen volume analysis because it provided only plaque volume. Figure 1 displays an overview of software interfaces used for the analysis of coronary artery plaque.

IVUS imaging protocol and analysis

A commercially available a 2.9-F, 40 MHz catheter (Boston Scientific/SCIMED, Minneapolis, Minnesota, or Volcano Corporation, Rancho Cordova, California) with axial resolution of ± 80 μm, lateral resolution of ± 200 μm) performed IVUS imaging throughout the length of the segment of interest after intracoronary nitroglycerine (100-200 μg). Images were acquired using a standard automated motorized pullback system

that permitted a cross-sectional area measurement at 0.5 mm/s with 30 frames per second.

An independent observer blinded to CCTA information analyzed IVUS images of lesion-containing target segments using commercially available computerized planimetry software (echoPlaque, INDEC Medical Systems Inc., Santa Clara, California). According to American College of Cardiology recommendations, atherosclerotic plaques were defined as structures located between the media and the intima with a thickness of at least 0.5 mm. Starting from the last frame toward the start frame of the target segment, cross sections spaced 0.5 mm apart were selected for analysis. The external elastic membrane (defined by the interface at the border between the media and the adventitia) and the lumen-intima interface were manually traced for each cross-sectional image. Atheroma (intima plus media) area for each cross section was calculated by subtracting the luminal area from the external elastic membrane cross-sectional area. Plaque volume per lesion was calculated from atheroma cross-sectional areas according to Simpson's rule. The location of target segments of coronary artery containing plaques were recorded with a landmark of side branches as a starting point and lesion lengths with the documentation of a downstream or upstream direction to make a reference for the locations measured during the process of plaque volume quantification using CCTA data.

Statistical analysis

Continuous variables of total plaque volume and lumen volume were presented as mean and 95% confidential interval compared using repeated

measure analysis of variance (ANOVA). Intraclass correlation coefficient (ICC) analysis was used to determine the degree of agreement among the results of the different software programs and IVUS results. A value of 0.05 or less was considered to indicate a statistically significant difference. Bonferroni correction was applied in a multiple comparison of repeated measures ANOVA. All analysis and graphs were performed using MedCalc software Version 16.1 (MedCalc Software, Mariakerke, Belgium).

Figure 1. An example of screen shots that provide an overview of software interfaces used for the automatic analysis of coronary artery plaque volume in a 79-year-old female patient: (A) Xelis by Infinitt, (B) Vitrea by Vital Images, (C) Advantage Workstation by GE Healthcare.

(A)

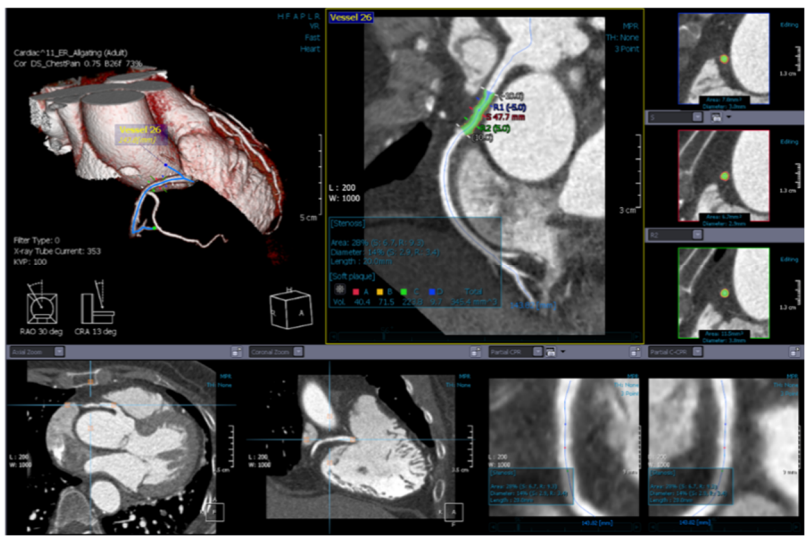

(B)

(C)

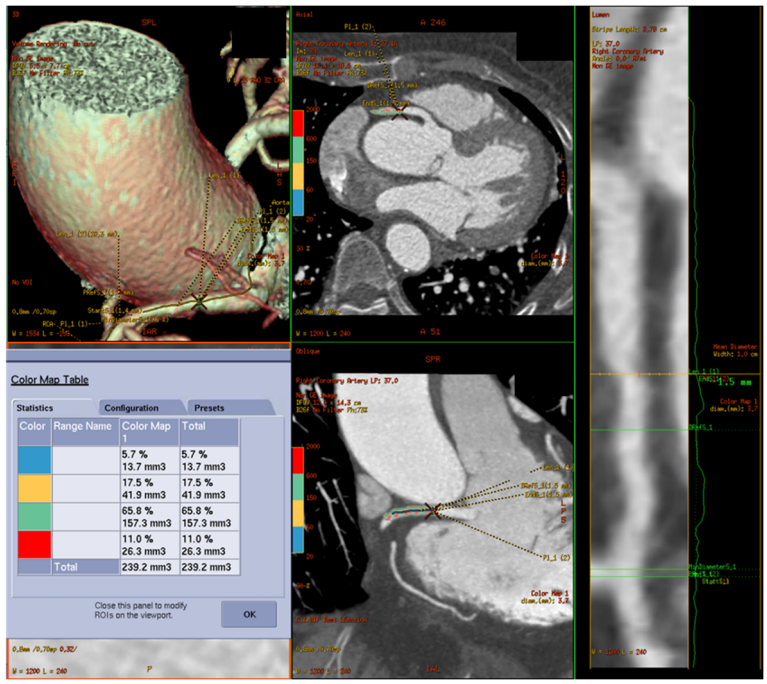
Color Map Table
Statistics
Configuration
Presets
Color
Range Name
Color Map 1
Total
5.7 %
13.7 mm3
5.7 %
13.7 mm3
17.5 %
41.9 mm3
17.5 %
41.9 mm3
65.8 %
157.3 mm3
65.8 %
157.3 mm3
11.0 %
26.3 mm3
11.0 %
26.3 mm3
Total
239.2 mm3
239.2 mm3
Close this panel to modify ROIs on the viewport.
OK

Part II. Phantom study

A vessel phantom was built with 25 tubular holes in a 5 cm thick polyethylene disc that was 15.2 cm in diameter (Figure 2). The diameter of each hole was 5 mm, 4.5 mm, 4 mm, 3.5 mm, 3 mm, and 2.9 mm to 1.0 mm with 0.1 mm intervals, simulating vessels of different diameters. The phantom was immersed in a mixture of an iodine contrast agent (Ultravist, Schering, Berlin, Germany) and saline, approximating attenuations of 600 HU at 100 kVp, with all tubular holes completely filled with a contrast mixture. CT scans were performed using three different kVps of 80, 100 and 120, five times in each protocol. All examinations were performed with a 320-row area detector CT scanner (Aquilion ONE, Toshiba Medical Systems, Tokyo, Japan) with a display field of view of 160 × 160 mm and a matrix size of 512 × 512, resulting in a pixel size of 0.31 mm. Slice thickness was 0.5 mm and reconstruction kernel was Cardiac FC03. Area-detector scanner was chosen instead of spiral multi-detector CT scanners used in CCTA clinical data acquisition in the Part I and Part IV studies. This was done to totally exclude table motion function because the hole diameters were very small and susceptible to any trace of motion.

Dedicated software (Xelis, Infinitt Healthcare, Seoul, Korea) measured the intraluminal attenuation of each hole. The center line of each tubular hole was semi-automatically selected and the attenuation was measured at every pixel through the center line. Intraluminal attenuation was calculated as the average attenuation of nine pixels (three by three pixels) around the center line pixel to indicate a square-shaped region of interest (ROI)

of 0.93 mm in length and 0.68 mm^2 in area. Data processing and analyses were performed using Microsoft Excel 2013 (Microsoft Corporation, Redmond, Washington).

Figure 2. A photo of the vessel phantom. A vessel phantom was built with 25 tubular holes in a 5 cm thick polyethylene disc with a 15.2 cm diameter.

Part III: Development of outer vessel segmentation algorithm

Outer vessel segmentation algorithm was developed as a working program in the Part IV study. Key steps for vessel segmentation were the initial centerline extraction, followed by curved planar reformation, perpendicular plane generation along the initial centerline, vessel outer boundary determination and tuning, and final center line determination.

Initial segmentation and initial center line extraction

Initial segmentation was obtained using a region-growing method which is a procedure that groups pixels into larger regions based on predefined growth criteria (28). The basic approach starts with a set of seed points and grow regions by appending each seed to neighboring pixels that have specific ranges of attenuation similar to the seed (28).

It started from a selection of the start and end points of the vessels of interest which served as seed points by clicking a cursor on a three-dimensional volume rendering image of the target segment. A crowd tubular segment was created between these two user-supplied seed points by allowing the point voxels propagating to nearby voxels with similar HU until reaching a minimum level of 250 HU. This threshold was considered adequate for these voxels to remain within the coronary artery lumen given that extraluminal epicardial fat is typically minus HU and reported CT attenuation values for noncalcified plaques (especially fibrous plaques) ranged from 70 ± 21 HU to 121 ± 43 HU (16,17,20,38-44).

The initial center line was extracted with the adoption of a minimum

cost path approach for dynamic programming. In this work a minimum cost path approach of dynamic programming was adopted to extract coronary artery centerlines from CTA data. The algorithm depends on the manual definition of the start and end point of the vessel. The cost image used in the minimal cost path approach is based on a vesselness measure and a smooth window function on attenuation.

Creation of curved planar reformation (CPR)

To generate longitudinal cross section displaying the lumen, wall and surrounding tissue of the vessel in a single image, curved planar reformatted image was made along the initial center line because vessels cannot be visualized completely throughout their entire course in an axial or orthogonal multiplanar reformation due to the natural curved course of vessels. CPR was reconstructed from the initial centerline using trilinear interpolation and set to be rotated interactively by users through 360° around the center line.

Perpendicular plane generation along the initial center line

Intersections perpendicular to the direction of the initial center line were generated on CPR image. A perpendicular plane was created serially for each voxel composing the initial center line without a gap on the path. Voxels on a perpendicular plane were supersampled using trilinear interpolation for enhancement of the spatial resolution.

The size of the x/y axes on the original axial image plane are approximately 0.3 mm for spatial resolution and ranged from 0.26 mm to 0.39 mm as determined by the display field of view (FOV) ranging from 14 cm to

20 cm for CCTA based on a 512 × 512 matrix that was a routine reconstruction matrix of current CT scans. With this original spatial resolution, only over hundred pixels account for the cross-section of a coronary artery that had a typical diameter of 3 mm to 4 mm. This condition has a relatively larger size and smaller number of pixels relative to the vessel size; however, it can cause averaging artifacts and represents an important cause of over- or underestimation in the quantification of atherosclerosis parameters such as lumen volume or plaque volume. This relatively low resolution data were up-sampled and resulted in a higher resolution using trilinear interpolation. Thereafter, the pixel size of the x/y axes decreased 0.05 mm to 0.15 mm and resulted in a vessel with approximately 1500 pixels per perpendicular plane. Pixel size will vary in different cases because the original voxel size was different according to CT machines and display FOV. In-plane pixel size would be also potentially different because most vessels are not aligned orthogonal to the perpendicular plane and require the application of different spacing.

Determination of the coronary artery outer boundary and tuning

This process was composed of three stages: profile generation, rolling ball curve fitting on horizontal map, and refinement (Figure 3).

Each end point was connected after 360 lines were drawn from the initial center through 360° to a certain pixel showing 0 HU on a perpendicular plane. The 0 HU threshold was used because it has been commonly used to discriminate epicardial fat from the outer vessel boundary (29-31). The threshold was stepped up in 100 HU each and a profile of the outer vessel

boundary was created when leakage was present due to an adjacent vessel or artifact. Irregular shaped profiles were then transformed using a rolling ball curve fitting into crude circular morphology with smooth connection. On the horizontal map where a total of 360 radial lines was aligned horizontally in order with downward direction; in addition, the bleached area from leakage interpolation was removed with a rolling ball with a radius of 1 mm. Final tuning was performed using a convex hull algorithm that consisted of iteratively applying the hit-or-miss transform to a convex with basic structuring elements (28). Processes were repeated for the entire target vessel segment containing plaque.

Final center line determination

The initial center line of the segmented vessel was refined as the serial collection of centers of gravity at each cross section after the determination of the outer boundary. A center of gravity represents the point where all HU within the outer vessel boundary is concentrated.

This automated segmentation method was a part of prototype of a current commercial software (Xelis CT Cardiac Version 10, Infinitt Healthcare, Seoul, Korea).

HU value output into Microsoft Excel sheet

HU values of all voxels within outer boundary on each cross-section perpendicular to the final center line of carefully selected target segments were obtained for the easy application of a different threshold for segmentation of the inner vessel boundary (i.e. vessel lumen). They were then

exported to a Microsoft Excel sheet in which the number of figures in each row represented the voxel number of the corresponding cross-section; subsequently, the number of rows indicate the total number of the generated cross-section (Figure 4). HU values of the center line were also output to a Microsoft Excel sheet. Two datasets were exported in the same order, from the proximal to distal portion of the target segment. Microsoft Excel sheets were suited for calculation in both a scan-adaptive and location-adaptive threshold method with different thresholds for the inner lumen segmentation and calcified plaques as described in detail later.

Validation of the developed outer vessel segmentation method

Clinical CT data were analyzed to investigate whether the developed vessel segmentation algorithm is a technically successful method for the segmentation of coronary artery outer boundary as compared to the reference standard of IVUS-derived vessel volume. A total twenty-two target segments were analyzed and the demographic information was described in detail in Part IV.

Image data were transferred to a workstation equipped with the developed software (Xelis Cardiac, Research Version 1, Infinitt Healthcare, Seoul, Korea); in addition, the target segment was pointed to automatically generate its outer boundary volume. Careful attention made sure that the length and location of each analyzed segment were identical to those of IVUS based on the indicator generated from IVUS analysis. A paired *t* test compared the automatically generated vessel volume of target segments to IVUS. A value of 0.05 or less was considered to indicate a statistically significant

difference. An ICC and Bland-Altman plot of vessel volume between CCTA and IVUS was also obtained.

Figure 3. Determination of the coronary artery outer boundary and tuning. (A) Profile generation: 360 lines were drawn from the initial center to a certain pixel showing 0 HU through 360° on a perpendicular plane, and each end point was connected. The threshold was stepped up in 100 HU each and the profile of the outer vessel boundary was created when leakage was present due to adjacent vessels or artifact. (B) Rolling-ball curve fitting: Irregularly shaped profiles were transformed into crude circular morphologies with smooth connections using rolling-ball curve fitting. The bleached area from leakage interpolation was removed with a rolling ball with a radius of 1 mm on the horizontal map where a total of 360 radial lines was sequentially aligned horizontally with downward direction. (C) Refinement: Final tuning was performed using a convex hull algorithm that consisted of iteratively applying a hit or miss transform to a convex with the basic structuring elements.

(A)

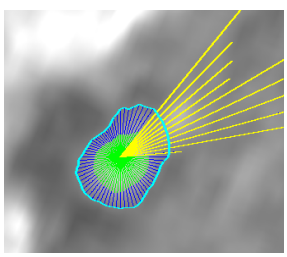

(B)

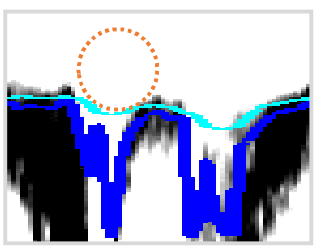

(C)

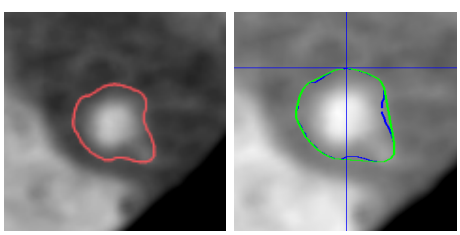

Figure 4. An example of a data sheet exported into Microsoft Excel from the newly developed vessel segmentation program. The number of rows is the total number of generated cross sections in a target segment. The number of cells in a row, except the first five cells, is the total number of voxels in a corresponding cross section. The first five cells consisted of one center Hounsfield unit, one blank cell, and three spacing information cells. The vessel area and lesion length can be calculated from the number of cells or rows and the spacing information.

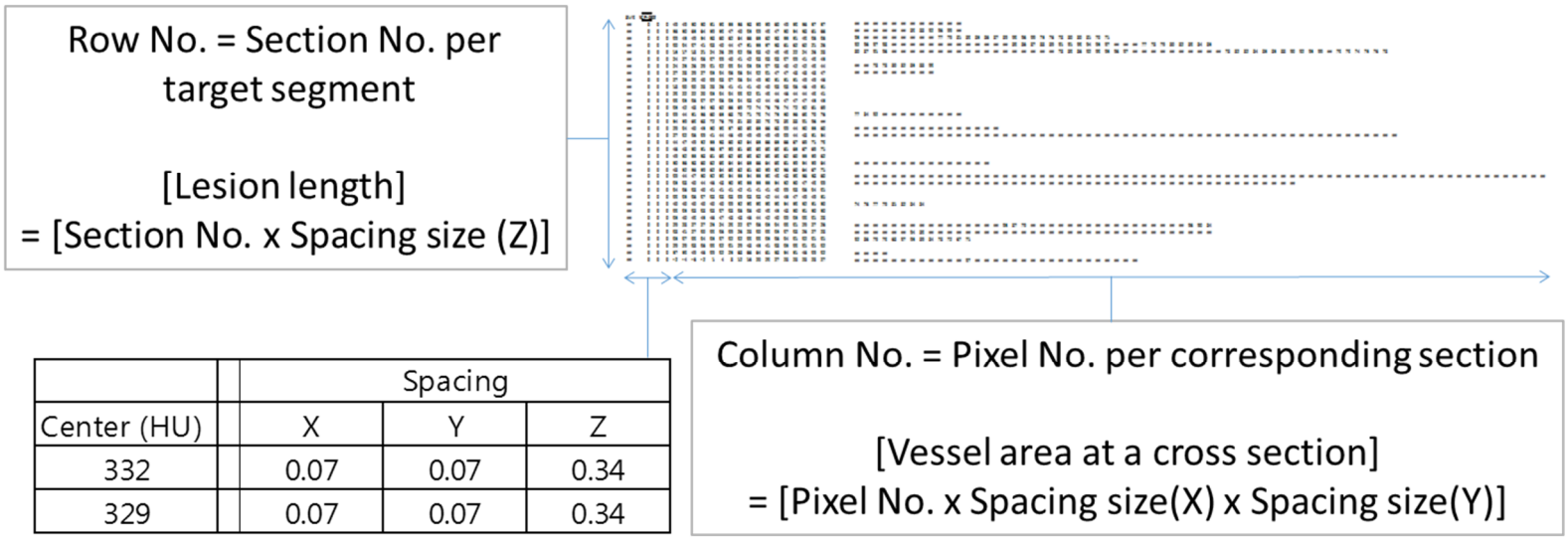

		Spacing		
Center (HU)		X	Y	Z
332		0.07	0.07	0.34
329		0.07	0.07	0.34

Part IV: A new concept for lumen segmentation and proof of concept

A new concept for luminal segmentation in plaque volume measurement

According to the phantom study result described in the result section, it can be expected that smaller diameter of the stenotic lumen causes a decreased intraluminal attenuation in the corresponding location compared to other locations showing a normal luminal diameter. Stenosis degree might be overestimated in commonly used threshold-based luminal segmentation methods in which the same attenuation threshold could be applied through the whole target vessel; consequently, plaque volume was also overestimated as plaque volume was calculated as vessel volume minus lumen volume. The lumen parameter was thought to be more accurately calculated if the stenotic location threshold decreased similar to the intraluminal attenuation. In the current study, the method that applies different thresholds at each location within a target segment is called the location-adaptive threshold method and the method of same attenuation threshold application through a target vessel is called the scan-adaptive threshold method. Figure 5 and Figure 6 illustrate the conceptual explanation and comparison of scan-adaptive as well as the location-adaptive threshold methods. A method that shows better agreement in coronary artery lumen volume quantification using a clinical data set was investigated for the validation of the new concept for a location-adaptive threshold method.

CCTA and IVUS data acquisition

Part I describes a detailed protocol of CCTA and IVUS data acquisition. Part I describes 30 target coronary artery segments in 25 patients; however, 8 segments were excluded because of suboptimal image quality due to motion artifact in the target segment on CCTA (n = 6) and failure of centerline extraction by the newly developed software algorithm (n = 2). Finally, 22 target segments in 15 patients (64.6 years; male, 80.0%) were enrolled in this proof of concept study. The number of target segments containing only noncalcified plaques were 7 and other segments were partly calcified plaque having a small portion of calcification.

CCTA data analysis

Thin section DICOM data sets were transferred to a dedicated workstation (Xelis Cardiac, Research Version 1, Infinitt Healthcare, Seoul, Korea). Center line extraction and vessel boundary were automatically analyzed. The starting and terminating points of each target segment containing a study lesion were carefully selected to match the corresponding landmark on IVUS. In this research version workstation, HU values of all voxels within the vessel boundary on each cross section were output to Microsoft Excel along with the HU value of the center of the corresponding cross section.

Segmented vessels contained lumen, noncalcified plaque and small part of calcified plaque. Therefore, two threshold values were required to discriminate noncalcified plaque, vessel inner lumen, and calcified plaque for the lumen volume quantification, and were defined as described below. Single threshold values were applied to differentiate noncalcified plaque from vessel

lumen for the analysis of noncalcified plaque segments in which calcified plaque did not exist.

Threshold definition in scan-adaptive method

The average CT values of the two lumens proximal and distal points to each target segment were measured and named as a scan-specific HU. Disease-free points were selected and round ROI were placed in the center of the lumen with a diameter approximately 50% of the lumen. For the determination of threshold between noncalcified plaque and inner lumen, 50% of the scan-specific HU was set according to the Full Width at Half Maximum (FWHM). The threshold to separate vessel inner lumen and calcified plaque was more than 110% of scan-specific HU because the standard deviation of the scan-specific HU was usually less than 10%; therefore, the number of pixels of inner lumen having over 110% of scan-specific HU was considered very small. The threshold value was the same at each cross section of the target segment.

Threshold definition in location-adaptive method

CT values at each point along the final centerline were exported to Microsoft Excel spreadsheets, and their derivatives were applied at each corresponding cross section as thresholds. A threshold of 50% of the centerline HU was used to distinguish between noncalcified plaque and inner lumen. A threshold of more than 110% of the centerline HU was used to distinguish between inner lumen and calcified plaque. These two threshold values were varied along the centerline position within a target segment.

Comparison of lumen volume and total plaque volume using scan-adaptive and location-adaptive methods

Each volume of three components of noncalcified plaque, lumen and calcified plaque at each cross section were calculated from the number of voxels of which the CT value met the corresponding range multiplying voxel spacing size after applying two thresholds. The sums of each of the three volumes in all cross sections indicated the total volume of noncalcified plaque, lumen and calcified plaque of the target vessel. Finally, lumen volume and total plaque volume (noncalcified plaque volume plus calcified plaque volume) were used for analysis.

Subgroup analysis according to the lumen size

Lumen volume measured by scan-adaptive and location-adaptive threshold methods would be more different in smaller lumen size because attenuation decreased as lumen size decreased according to the phantom study result. Therefore, subgroup analysis investigated whether the lumen size affected the difference of the lumen volume between scan-adaptive and location-adaptive threshold methods. Calcified plaque volume was calculated from pixel numbers that met the threshold range regardless of cross section location. Pixels that consist of lumen can be misclassified as calcified plaque because there exists only attenuation information without location information; therefore, only noncalcified plaque segments were included in the analysis because calcified plaque was mathematically excluded from this study.

IVUS datasets were modified to form subgroups. A frame obtained by IVUS was 1/60 mm, which differed from the section thickness, i.e., the z-spacing, of the CCTA, which varied from 0.26 mm to 0.32 mm, depending on the scan. Therefore, the IVUS frames were grouped according to the z-axis spacing of the corresponding CCTA, and the values of the lumen area measured by IVUS for every 15.6 to 19.2 frames were averaged and rounded to the nearest integer.

Based on these modified lumen area measured by IVUS equalized to CCTA section thickness, total cross sections of noncalcified plaque segments were divided into three subgroups of lumen size < 3 mm^2 (approximately 2 mm in lumen diameter), 3 mm^2-7 mm^2, and ≥ 7 mm^2 (approximately 3 mm in lumen diameter). The smallest subgroup with lumen size < 3 mm^2 was excluded because it was thought that lumen area was too small and was prone to errors even though there was only a trace degree of mismatch between the IVUS and CCTA cross-section.

Statistical analysis

Continuous variables of total plaque volume/area and lumen volume/area were presented as a mean and a 95% confidential interval then compared using repeated measure ANOVA or paired *t* test. Friedman test provided the volume analysis for the noncalcified plaque segments instead of repeated measure ANOVA due to the small number of cases. Bonferroni correction was applied in multiple comparison. ICC evaluated agreement between CCTA-derived and IVUS-derived results by applying the same raters for all subjects model and absolute agreement type. Bland-Altman analysis

was performed by plotting the mean against the difference in measurements (32). Limits of agreement were defined as the mean difference plus and minus 1.96 times the standard deviation of the differences for the upper and lower limits, respectively. A value of 0.05 or less was considered to indicate a statistically significant difference. All of the statistical analyses and graphing were performed using the MedCalc® software Version 16.1 (MedCalc Software, Mariakerke, Belgium).

Figure 5. Conceptual illustration of the scan-adaptive threshold method and location-adaptive threshold method. Three locations having different lumen areas and different attenuation profiles are generated when a vessel has two stenoses with a different degree. A uniform threshold is applied to all three locations in the scan adaptive threshold method (A).The lumen area at the location with mild stenosis (right) is underestimated and the lumen area at the severe stenosis (middle) is expressed as occlusion, whereas the lumen area at the location without stenosis (left) is shown correctly. In the location-adaptive threshold method (B), different threshold values are given to each location, according to attenuation profiles, and the lumen areas of all three locations can be calculated accurately.

(A)

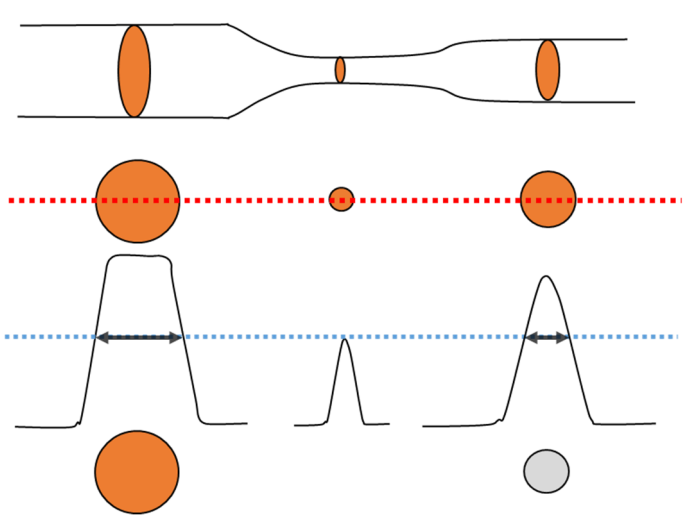

(B)

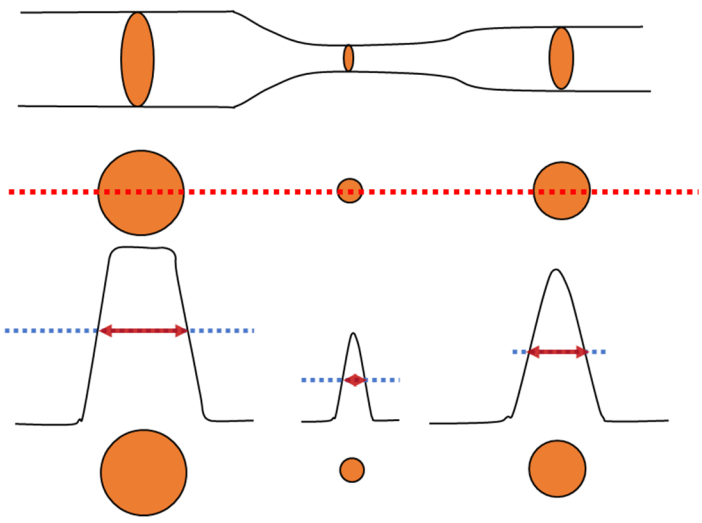

Figure 6. A simplified schematic example explaining difference between the scan-adaptive and location-adaptive threshold methods. Number within each cell is attenuation value of that cell. Cells with a black figure represent actual plaques versus cells with a colored figure that represent actual lumen. Cells with gray color indicate estimated plaques while cells with orange and yellow color indicate estimated lumen. The cross-section in right has smaller lumen due to stenosis while the cross-section in left has a larger lumen. In the scan-adaptive threshold method, the same threshold of 400 HU which is the half maximum attenuation value of the larger lumen is applied to both cross sections. Therefore, the lumen area might be underestimated at the stenotic location because cells showing 400 HU or more are only counted for lumen; however, cells that show an attenuation value between 250 HU and 400 HU are not regarded as lumen despite actual lumen. Note cells with gray color even with a colored figure. Threshold values are adjusted to each location in the location-adaptive threshold method with 400 HU in the right cross-section and 250 HU in the left cross-section. Then, mismatched cells shown in the cross section with stenosis when using scan-adaptive threshold method disappear and the lumen area is correctly calculated.

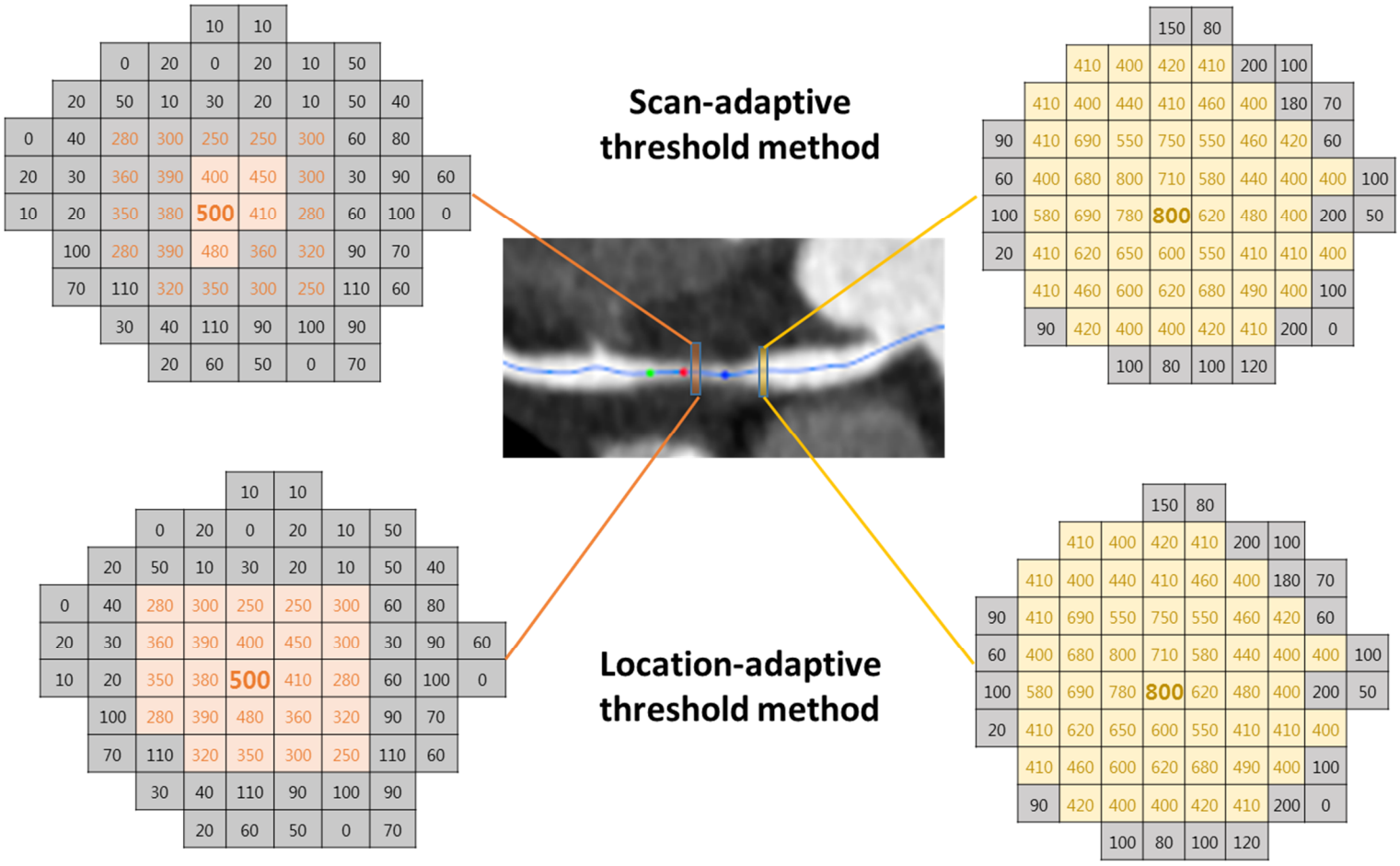
Scan-adaptive threshold method
Location-adaptive threshold method

Results

Part I: Interplatform reproducibility of plaque volume and lumen volume

Table 1 presents the mean value and 95% confidence interval (CI). For total plaque volume, ICCs among the values provided by automated software programs were low and ranging from 0.369 to 0.482; in addition, the ICC between the value derived from each software and IVUS ranged from 0.453 to 0.571 (Figure 7A). ICC was 0.759 between the lumen volume measured by Xelis and AWS software (Figure 7B). Figure 8 presents the bar plotting graphs of total plaque volume and lumen volume.

Table 1. Automated Volumetric Data for Each Software Program and IVUS

	Total plaque volume (mm^3)	Lumen volume (mm^3)
IVUS	108.5 (84.4 to 132.5)	96.9 (69.4 to 124.4)
Xelis	76.1 (48.8 to 103.5)	143.8 (106.5 to 181.1)
AWS	115.7 (86.4 to 145.1)	164.9 (124.5 to 205.3)
Vitrea	167.2 (128.2 to 206.2)	-

Data are means. Data in parentheses are 95% confidence interval. IVUS = intravascular ultrasound.

Figure 7. Bar graphs showing low interplatform reproducibility among commercially available coronary plaque quantification programs. The mean values and 95% confidence intervals of the plaque volume (A) and lumen volume (B) are shown. The values on the horizontal lines above the bars indicate interclass correlation coefficients between the two values at the ends of each line.

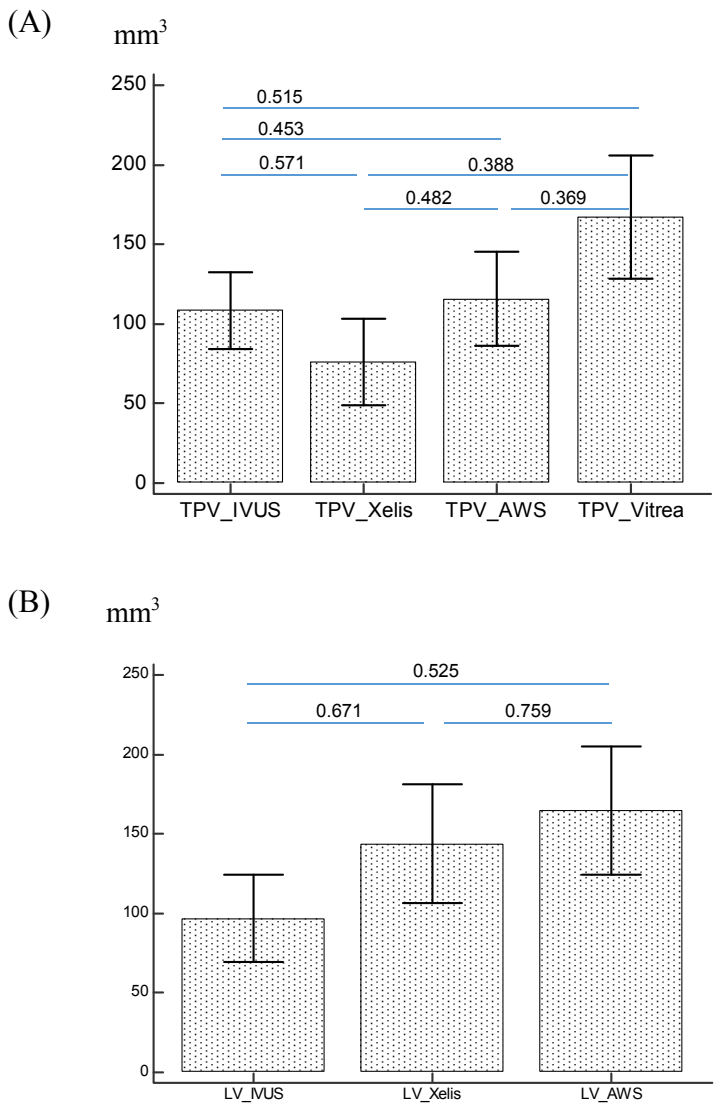

Figure 8. Bar plotting graphs of total plaque volume (A) and lumen volume (B) measured by different automated software programs for coronary plaque volume quantification and IVUS.

(A)

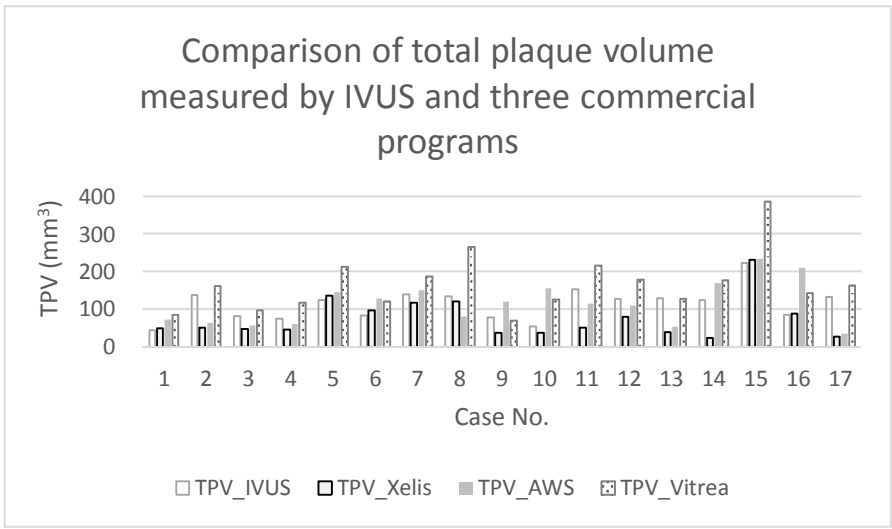

(B)

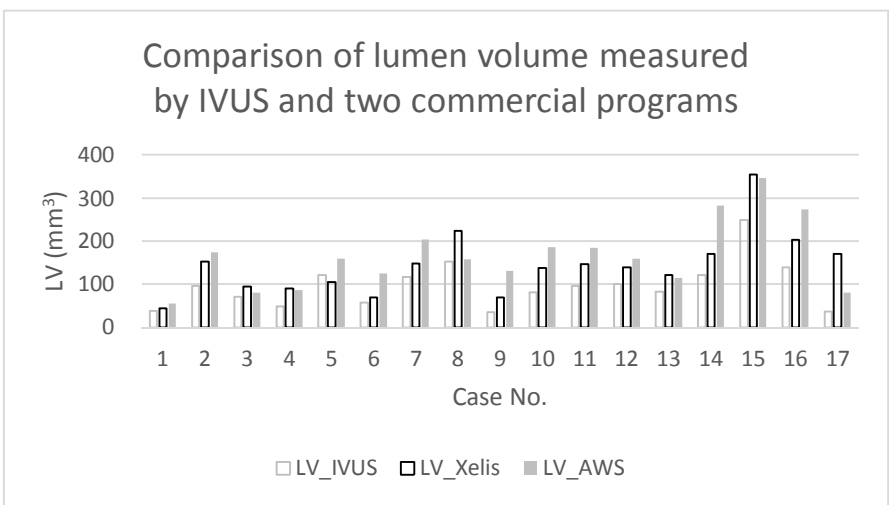

Part II: Vessel phantom study

All holes were filled with the same contrast mixture; however, intraluminal attenuation was observed to gradually decline along with the decreased diameter of the holes (Figure 9, Figure 10). The reduction of intraluminal attenuation was also greater as the diameters decreased. The same findings were also observed irrespective of the tube voltage used. Table 2 provides detailed attenuation values.

Table 2. Detailed Attenuation Values According to the Hole Size

Hole size (mm)	Attenuation (HU)		
	80 kVp	100 kVp	120 kVp
5.0	810.5	612.7	483.8
4.5	786.8	593.2	469.1
4.0	759.3	572.7	454.4
3.5	706.4	538.7	434.0
3.0	646.1	490.4	400.8
2.9	622.7	482.9	395.0
2.8	601.4	466	381.6
2.7	591.5	452.5	374.3
2.6	574.2	439.7	363.2
2.5	559.7	418.6	351.8
2.4	535.6	407.7	345.2
2.3	516.6	391.9	336.7
2.2	497.1	370.6	318.3
2.1	473.5	361.1	310.3
2.0	448.0	347.4	288.1
1.9	414.7	328.8	275.9
1.8	387.9	304.8	260.5
1.7	326.8	275.3	235.5
1.6	312.1	245.4	202.1
1.5	272.9	229.2	192.5
1.4	238.3	196.7	168.9
1.3	195.8	178.9	136.4
1.2	160.7	144.8	109.9
1.1	132.4	111.7	92.7
1.0	98.7	88.3	68.0

Figure 9. CT image of the vessel phantom. A vessel phantom was immersed in a mixture of an iodine contrast agent and saline, with all tubular holes completely filled with the contrast mixture.

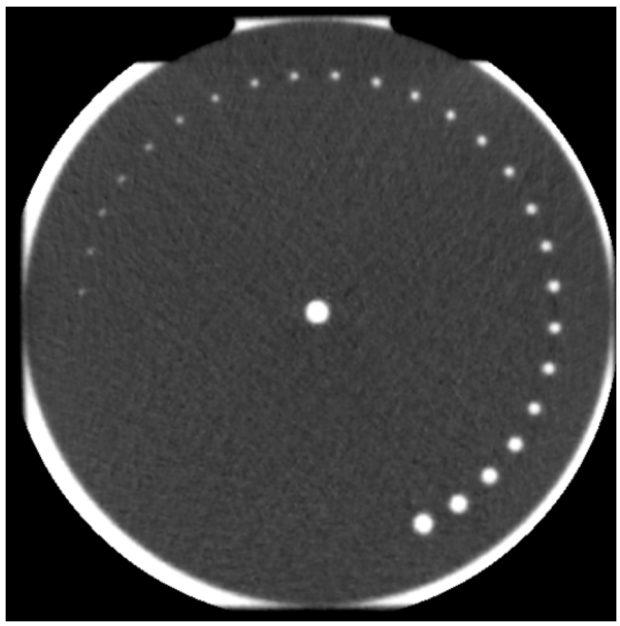

Figure 10. Decrease in attenuation with diminution of vessel size. Intraluminal attenuation decreased as the diameter diminished irrespective of the tube voltage used.

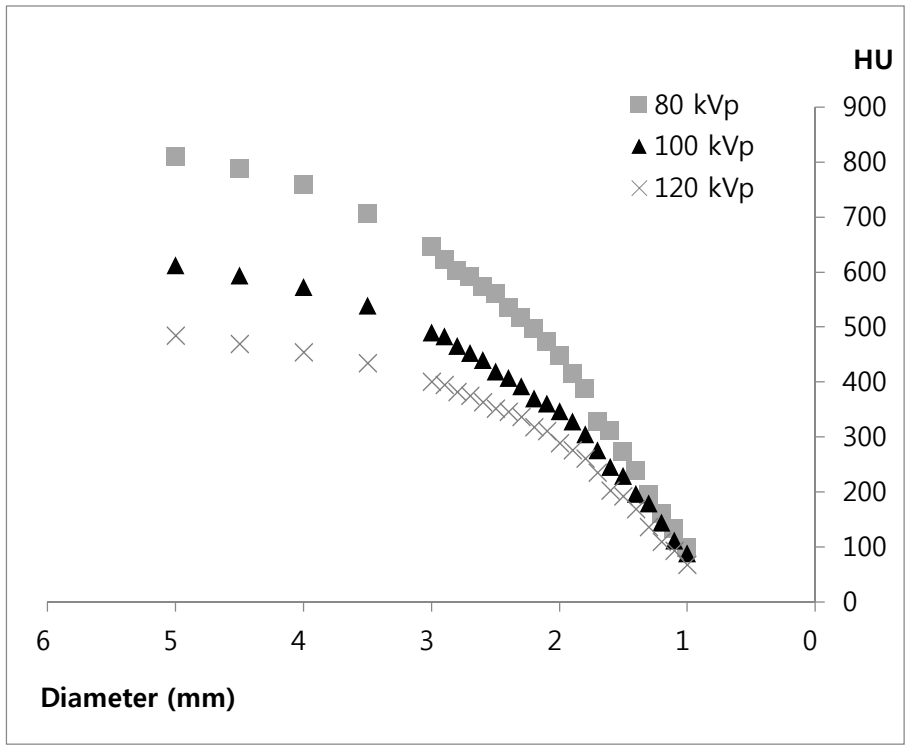

Part III: Validation of a developed software for outer vessel boundary segmentation

Mean vessel volume measured by CCTA-using software and IVUS were 219.5 mm^3 (95% CI, 167.6 to 271.4 mm^3) and 207.4 mm^3 (95% CI, 163.8 to 251.0 mm^3), respectively (P = 0.202) (Figure 11A). The studied method and standard reference showed excellent agreement in the vessel volume measurement with an ICC of 0.919 (95% CI, 0.817 to 0.965). The limit of agreement showed -96.2 mm^3 to 72.1 mm^3 without a significant systemic bias (Figure 11B) on Bland-Altman plot.

Figure 11. Comparison between IVUS and new software algorithm using CCTA for assessment of vessel volume. The bar graph (A) shows no significant difference in vessel volume as measured by IVUS (mean = 207.4 mm^3) and the new software algorithm using CCTA (mean = 219.5 mm^3). On Bland-Altman plot (B), there was no systemic bias and most cases were within the limit of agreement.

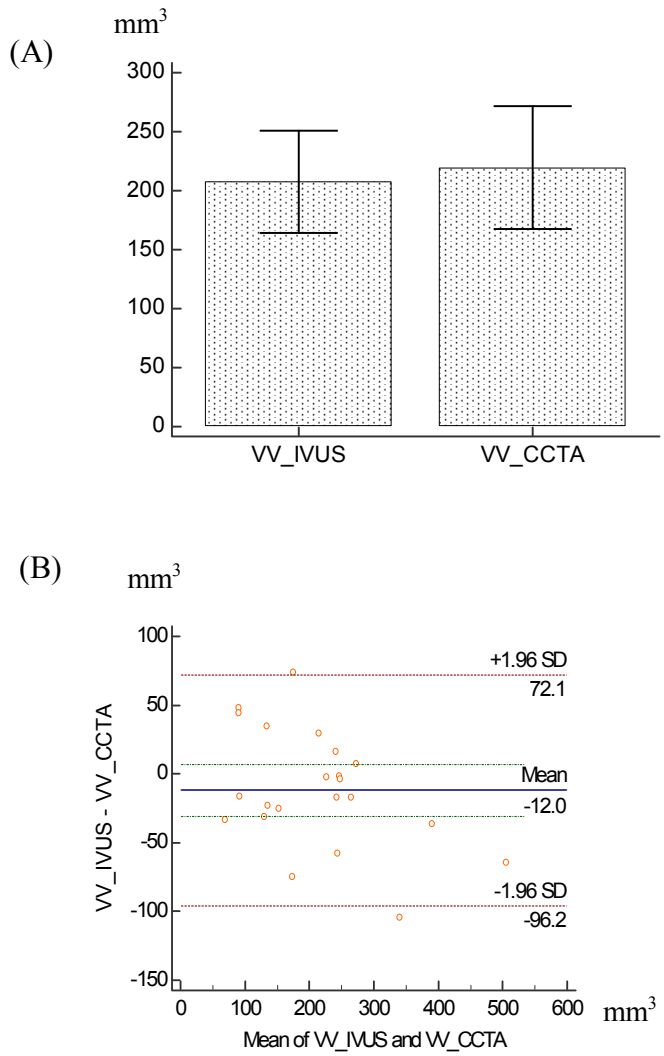

Part IV: Validation of location-adaptive threshold method as a new concept for lumen segmentation

Comparison of lumen volume and total plaque volume measured by two different threshold methods and IVUS

Mean values of lumen volume measured by IVUS, scan-adaptive and location-adaptive methods were 96.0 mm^3 (95% CI, 70.0 mm^3 to 116.2 mm^3), 78.4 mm^3 (95% CI, 57.2 mm^3 to 99.6 mm^3) and 93.7 mm^3 (95% CI, 73.0 mm^3 to 114.5 mm^3), respectively (Figure 12). There was a significant difference between the lumen volumes measured by IVUS and that measured by the scan-adaptive method ($P = 0.0152$); however, the lumen volumes measured by IVUS and the location-adaptive method were not significantly different ($P = 0.999$). The lumen volume measured by the scan-adaptive method was significantly smaller than that measured by the location-adaptive method ($P < 0.0001$). ICCs of the lumen volume as determined by IVUS versus the two CCTA-derived values based on the scan-adaptive and location-adaptive methods were 0.872 (95% CI, 0.609 to 0.952) and 0.930 (95% CI, 0.840 to 0.971), respectively. On Bland-Altman plots for lumen volumes measured by IVUS and scan-adaptive method, a systemic bias was noted and the mean difference between the lumen volume of IVUS and scan-adaptive method was 14.6 mm^3 (95% CI, 4.9 mm^3 to 24.3 mm^3) ($P = 0.005$); however, there was no systemic bias between lumen volumes measured by IVUS and the location-adaptive method with a mean difference of -0.73 mm^3 (95% CI, -9.14 mm^3 to 7.69 mm^3) ($P = 0.859$) (Figure 13). Figure 14 provides scatter diagrams of the lumen volume.

For the total plaque volume, the means measured by IVUS, the scan-adaptive and location-adaptive methods were 114.4 mm^3 (95% CI, 90.7 mm^3 to 138.1 mm^3), 141.1 mm^3 (95% CI, 107.0 mm^3 to 175.1 mm^3) and 125.7 mm^3 (95% CI, 93.5 mm^3 to 158.0 mm^3), respectively. The total plaque volume measured by the scan-adaptive method was significantly larger than that obtained by IVUS ($P = 0.0142$) and by the location-adaptive method ($P < 0.0001$).There was no significant difference between the total plaque volume measured by IVUS and by the location-adaptive method ($P = 0.547$). The ICCs of the lumen volume between IVUS and two CCTA-derived values obtained by the scan-adaptive and location-adaptive methods were 0.766 (95% CI, 0.396 to 0.907) and 0.813 (95% CI, 0.606 to 0.917), respectively. Figure 15 and Figure 16 show Bland-Altman plots and scatter diagrams for total plaque volume, respectively.

Results of analysis of noncalcified plaque segments

For noncalcified plaque segments ($n = 7$), Friedman test detected a significant difference between the lumen volume measured by IVUS and the scan-adaptive method ($P < 0.05$). There were no significant differences between the lumen volume measured by IVUS and the location-adaptive method or between the location-adaptive and scan-adaptive method ($P > 0.05$). On Bland-Altman analysis, 95% limits of agreement were narrow and ranged from -17.5 mm^3 to 33.7 mm^3 without significant systemic bias in the location-adaptive method compared to IVUS; however, the scan-adaptive method showed wider 95% limits of agreement that ranged from -24.4 mm^3 to 68.8 mm^3 as well as a positive systemic bias of IVUS-derived lumen volume

(Figure 17). ICCs between lumen volume measured by IVUS and each scan-adaptive and location-adaptive method were 0.817 (95% CI, 0.053 to 0.969) and 0.945 (95% CI, 0.634 to 0.991), respectively. Figure 18 displays the scatter diagrams.

Results of subgroup analysis

Table 3 presents the mean values and the 95% CIs for the calculated lumen area according to the lumen size based on the reference standard. Mean values of lumen areas for the 314 cross-sections ($\geq$ 3 mm^2) were 6.47 mm^2, 5.00 mm^2, and 5.67 mm^2 in IVUS, scan-adaptive method, and location-adaptive method, respectively ($P < 0.001$ in all comparisons). ICCs between IVUS and the scan-adaptive and location-adaptive methods were 0.614 (95% CI, 0.173 to 0.798) and 0.668 (95% CI, 0.432 to 0.792) for scan-adaptive and location-adaptive methods, respectively. Bland-Altman analysis indicated that the limit of agreement was narrower in the location-adaptive method (-1.9 mm^2 to 3.5 mm^2) than in the scan-adaptive method (-1.9 mm^2 to 4.8 mm^2) compared to the reference standard (Figure 19). Figure 20 displays the scatter diagrams.

In the lumen size group that was between 3 mm^2 and 7 mm^2 (n= 202), the mean values of the lumen areas were: IVUS 5.38 mm^2, scan-adaptive method 3.85 mm^2, and location-adaptive method 4.92 mm^2, respectively ($P <$ 0.001 in all comparisons) (Figure 21, Figure 22). ICCs based on IVUS was 0.334 (95% CI, 0.027 to 0.550) and 0.348 (95% CI, 0.211 to 0.469) for scan and location-adaptive methods, respectively. Bland-Altman plots indicated that the location-adaptive method showed narrower limits of agreement than

the scan-adaptive method (Figure 23).

In the larger lumen group with lumen size ≥ 7 mm^2 (n = 112), the mean values of lumen area according to the scan-adaptive (7.09 mm^2, 95% CI: 6.67 mm^2 to 7.50 mm^2) and location-adaptive (7.01 mm^2, 95% CI: 6.69 mm^2 to 7.34 mm^2) method were not significantly different (P = 0.336) (Figure 24 and Figure 25). But, the mean value measured by IVUS (8.43 mm^2, 95% CI: 9.17 mm^2 to 8.69 mm^2) was significantly larger than those measured by both two methods (P < 0.0001). ICCs were 0.555 (95% CI, 0.068 to 0.775) and 0.544 (95% CI, -0.071 to 0.805) for scan-adaptive and location-adaptive methods versus the IVUS value, respectively. Figure 26 presents the Bland-Altman plots.

Table 3. Subgroup Analysis of Lumen Area Measured by Scan-adaptive and Location-adaptive Threshold Methods According to the Lumen area Based on the Reference Standard.

	Lumen area (mm^2)		
Lumen area on IVUS	IVUS	Scan-adaptive method	Location-adaptive method
Total (n = 314)	6.47 (6.25 to 6.68)	5.00 (4.70 to 5.30)	5.67 (5.47 to 5.86)
3-7 mm^2 (n = 202)	5.38 (5.21 to 5.55)	3.85 (3.54 to 4.15)	4.92 (4.75 to 5.09)
$\geq$ 7mm^2 (n = 112)	8.43 (8.17 to 8.69)	7.09 (6.67 to 7.50)	7.01 (6.69 to 7.34)

Data are means. Data in parentheses are 95% confidence interval. IVUS = intravascular ultrasound.

Figure 12. Comparison of lumen volume measured by IVUS and scan-adaptive and location-adaptive threshold method. The mean values of the lumen volume were 96.0 mm^3, 78.4 mm^3, and 93.7 mm^3 for IVUS, the scan-adaptive threshold method, and the location-adaptive threshold method, respectively (n = 22).

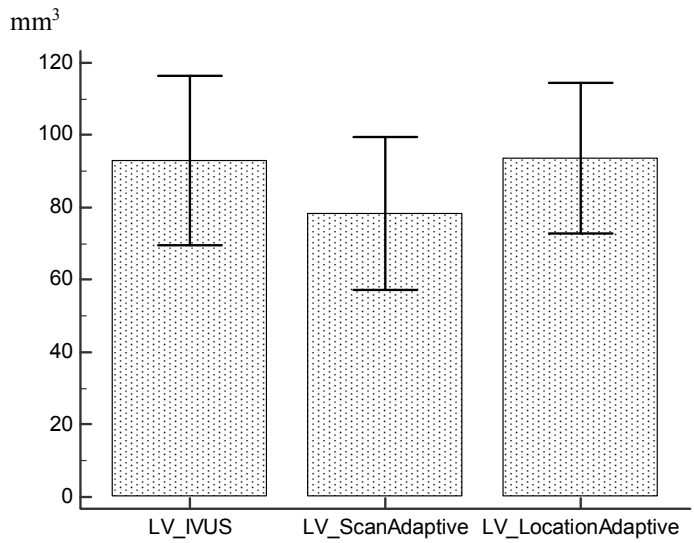

Figure 13. Bland–Altman analysis for lumen volume. Comparison between the values measured by IVUS and the scan-adaptive threshold method (A) as well as a comparison between the values measured by IVUS and the location-adaptive threshold method (B) are shown. The limit of agreement was narrower and there was no systemic bias when the location-adaptive threshold method was applied.

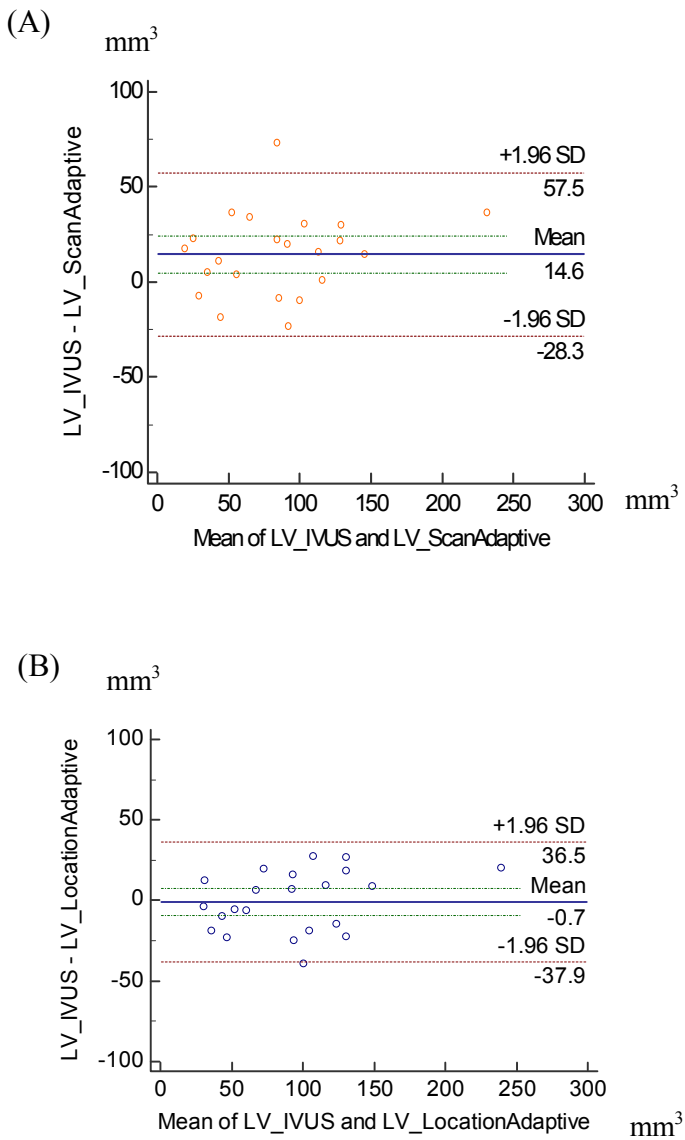

Figure 14. Scatter diagrams for lumen volume in the application of different methods compared to IVUS. *Dashed line = line of equality*

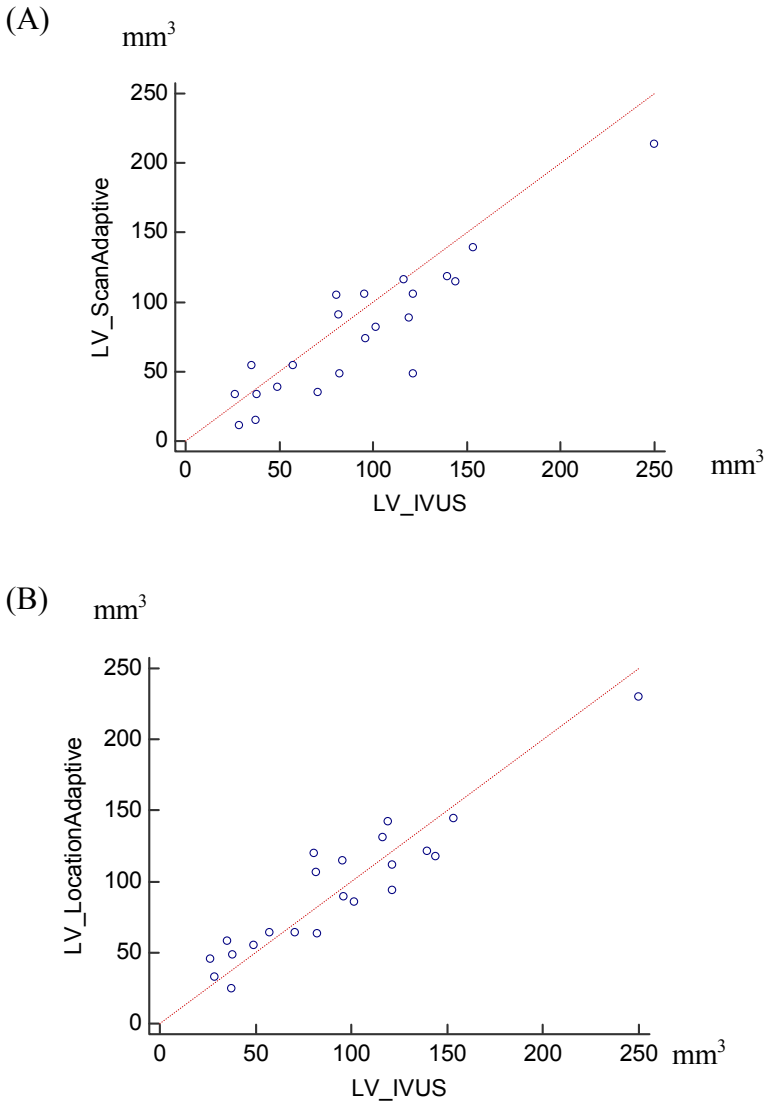

Figure 15. Bland-Altman analysis for total plaque volume. Systemic bias (overestimation) was noted with the scan-adaptive threshold method (A), whereas there was no systemic bias with the location-adaptive threshold method (B), compared to IVUS.

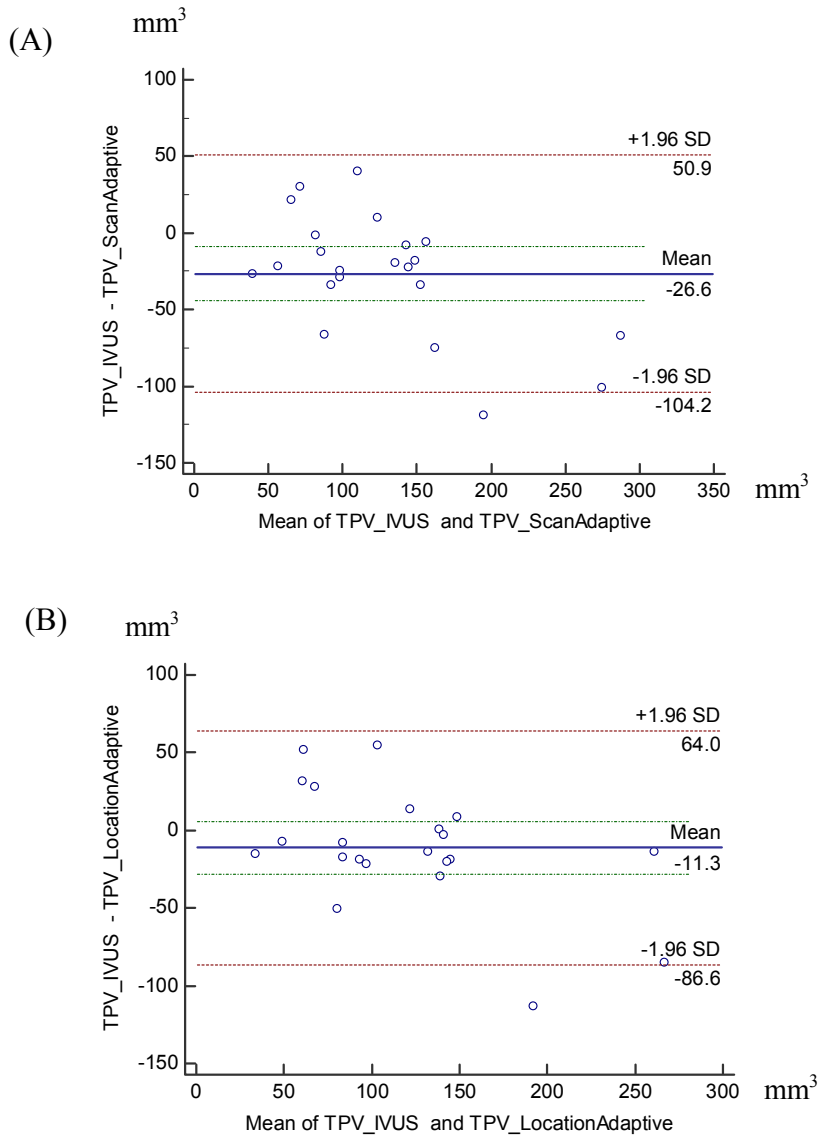

Figure 16. Scatter diagrams for total plaque volume in the application of different methods compared to IVUS. *Dashed line = line of equality*

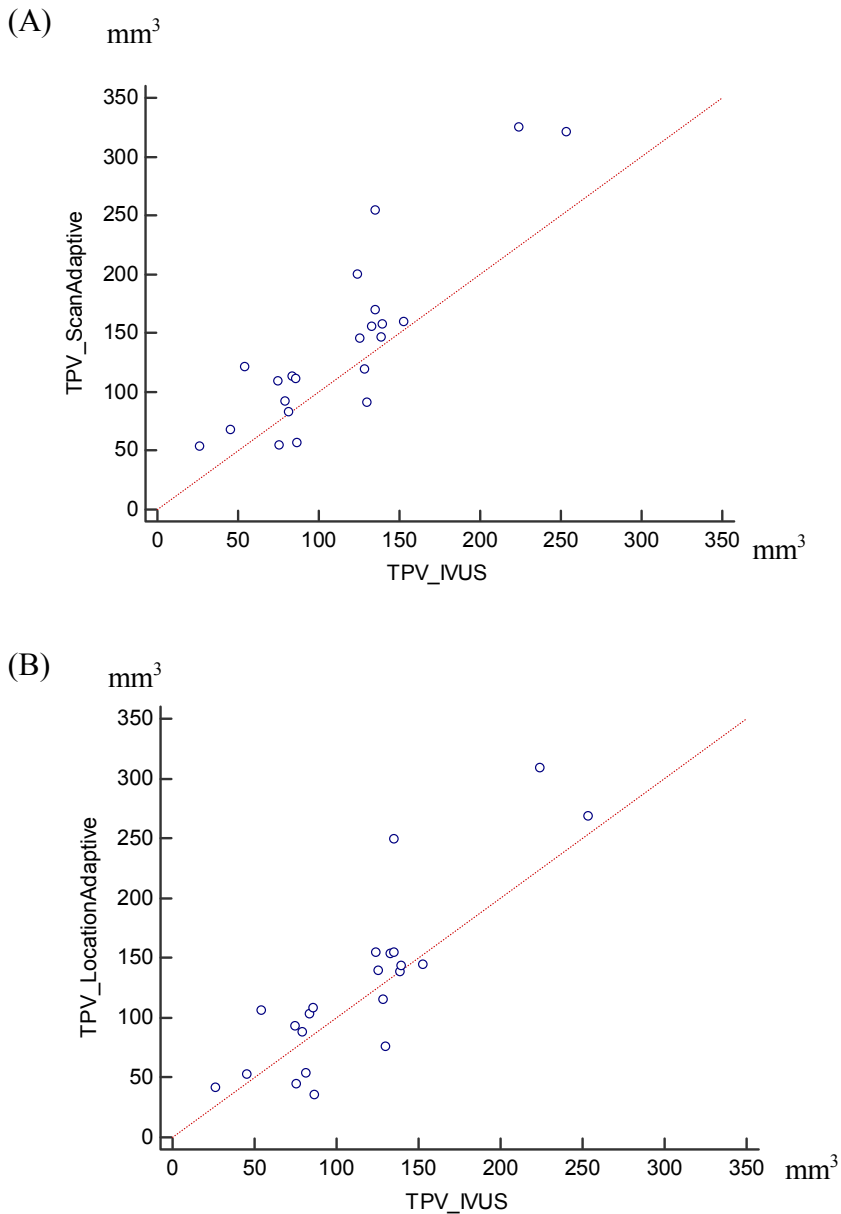

Figure 17. Bland-Altman analysis for lumen volume in noncalcified plaque segments. Negative systemic bias for lumen volume was noted with the scan-adaptive threshold method, in comparison to IVUS (A). The 95% confidence interval of the difference in lumen volume ranged from 0.2 to 44.2 mm^3. However, there was no systemic bias and a narrower limit of agreement was noted in the location-adaptive threshold method (B).

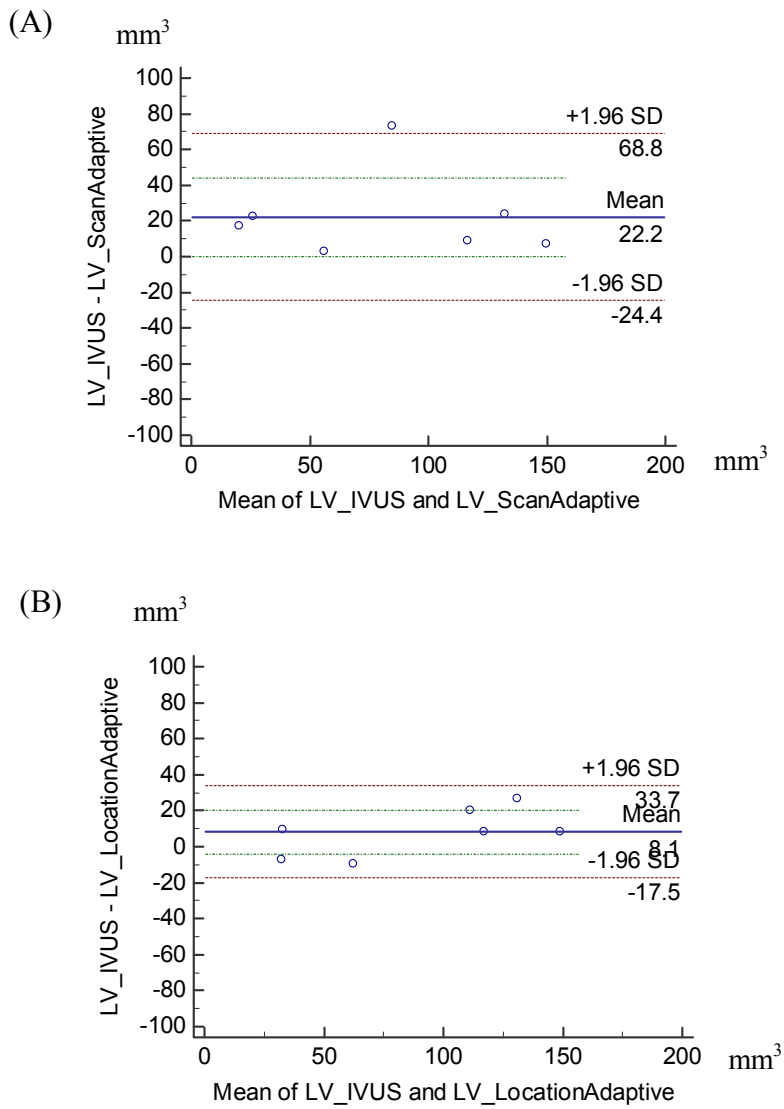

Figure 18. Scatter diagrams of lumen volume in noncalcified plaque segments. *Dashed line = line of equality*

(A)

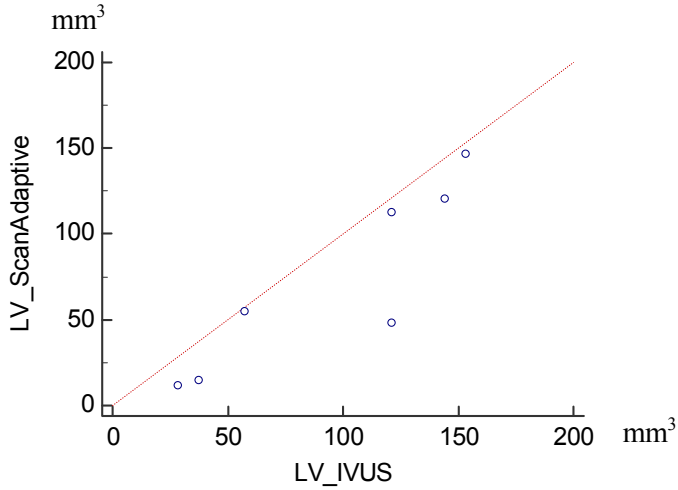

(B)

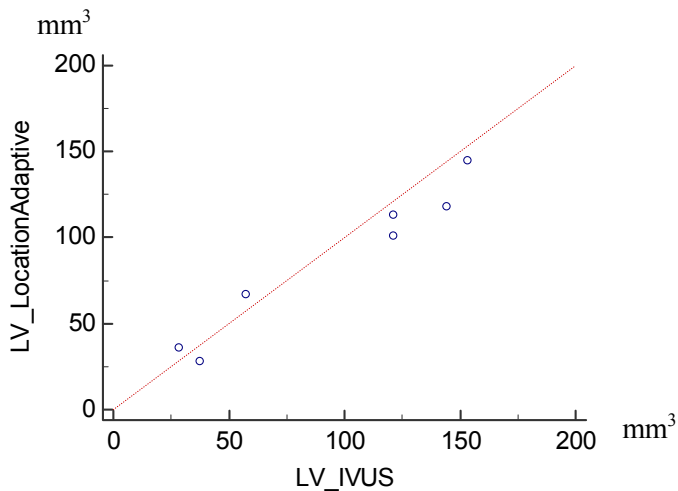

Figure 19. Bland-Altman analysis for lumen area in subgroup analysis.

Cross sections with a lumen area of 3 mm^2 or more were analyzed (n = 312).

(A)

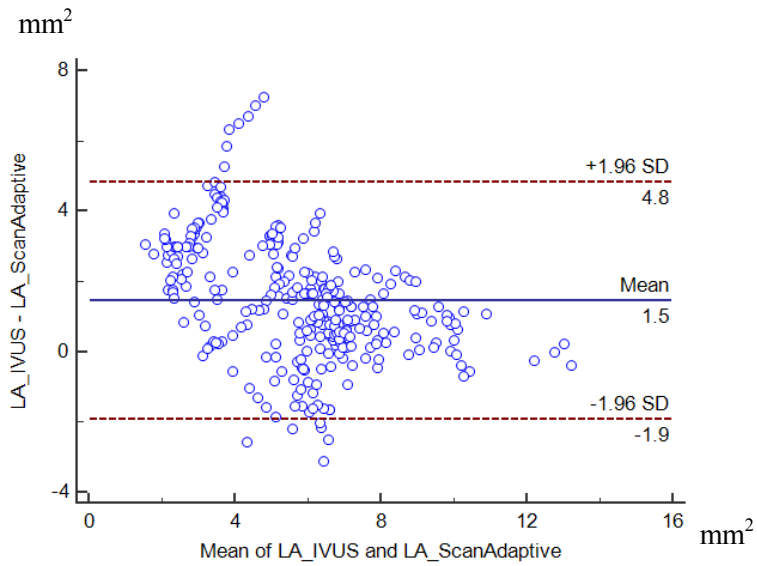

(B)

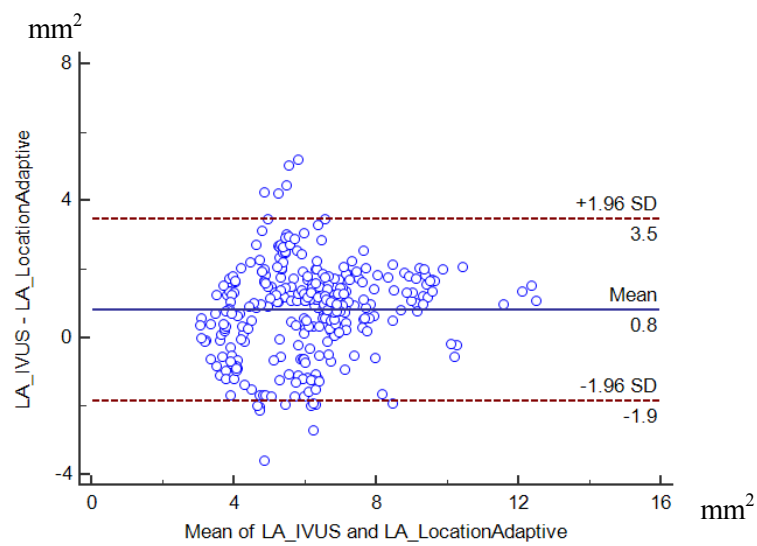

Figure 20. Scatter diagrams of lumen area in subgroup analysis. Lumen areas determined by scan-adaptive (A) and location-adaptive (B) threshold methods were plotted according to the actual lumen area (≥ 3 mm^2) based on a reference standard using IVUS. A comparison between location-adaptive and scan-adaptive threshold methods (C) indicated a significant underestimation of lumen area that was noted in the range of less than 6 mm^2.

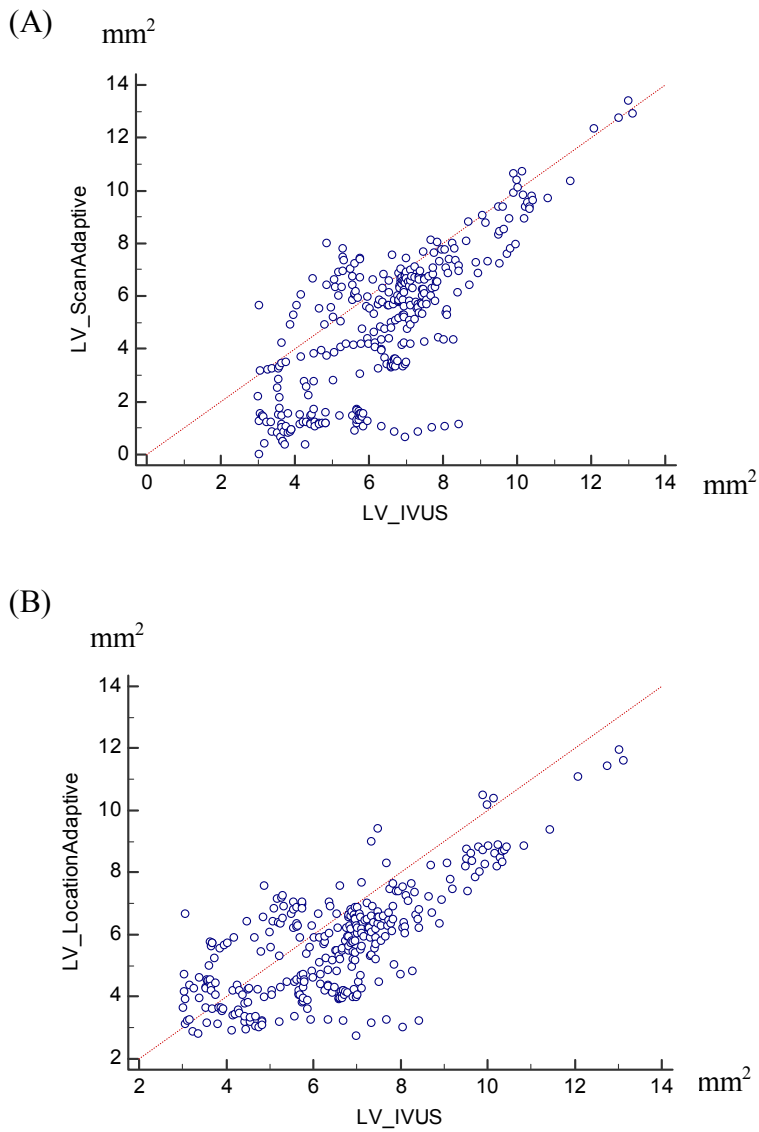

(C)

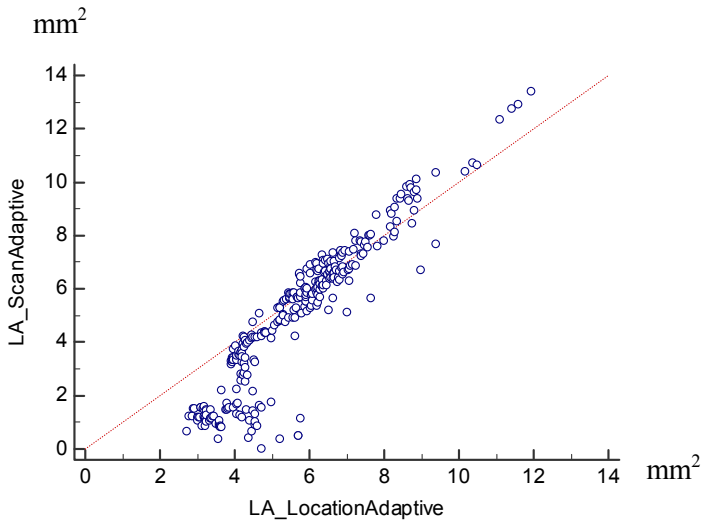
mm2
14
12
10
8
6
4
2
0
LA_ScanAdaptive
0
2
4
6
8
10
12
14
mm2
LA_LocationAdaptive

Figure 21. Comparison of lumen area in a subgroup with a lumen area between 3-7 mm^2. There were significant differences among three methods (n = 202).

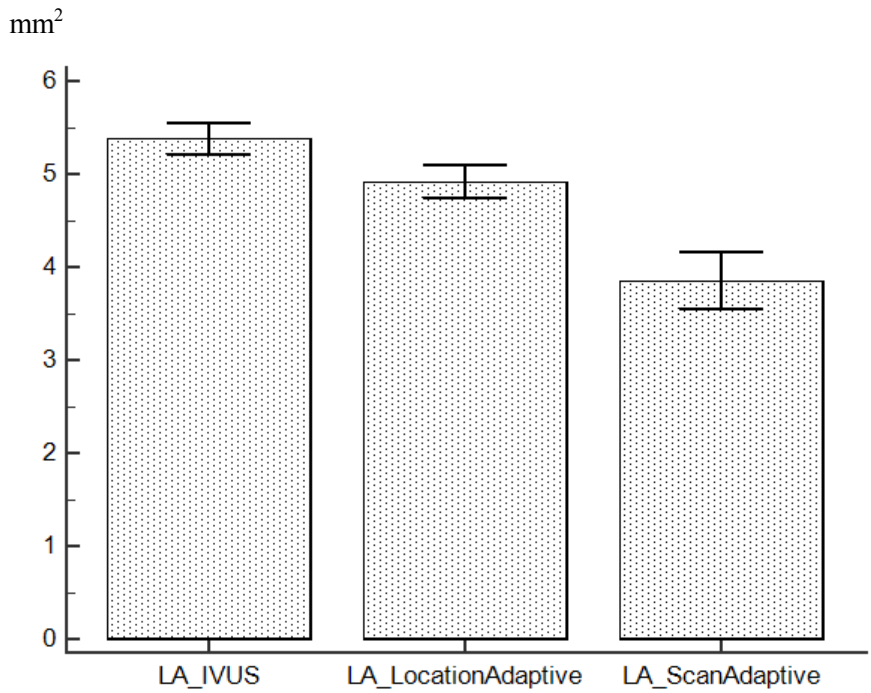

Figure 22. An example of comparison of scan-adaptive and location-adaptive threshold methods for lumen area measurement for a segment with small luminal area in a 76-year-old male patient. The thickness of each cross section was 0.36 mm, and the total length of the target segment was 7.8 mm. The lumen area, measured by the reference standard, was 3-4 mm^2. The lumen area calculated using the scan-adaptive threshold method was significantly smaller than that determined by the reference standard, whereas that calculated using the location-adaptive threshold method was slightly smaller or larger.

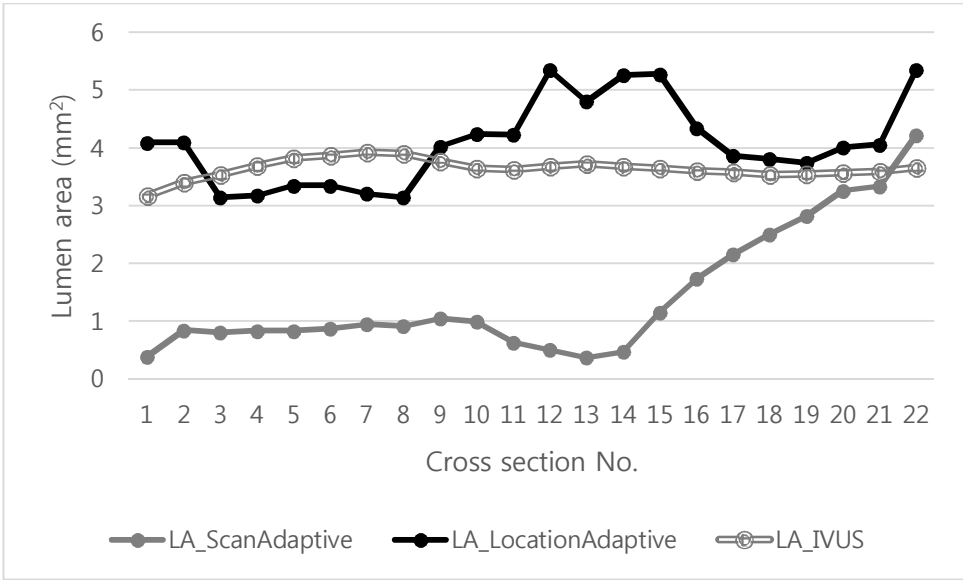

Figure 23. Bland-Altman plot for lumen area in a subgroup with a lumen area of 3-7 mm^2.

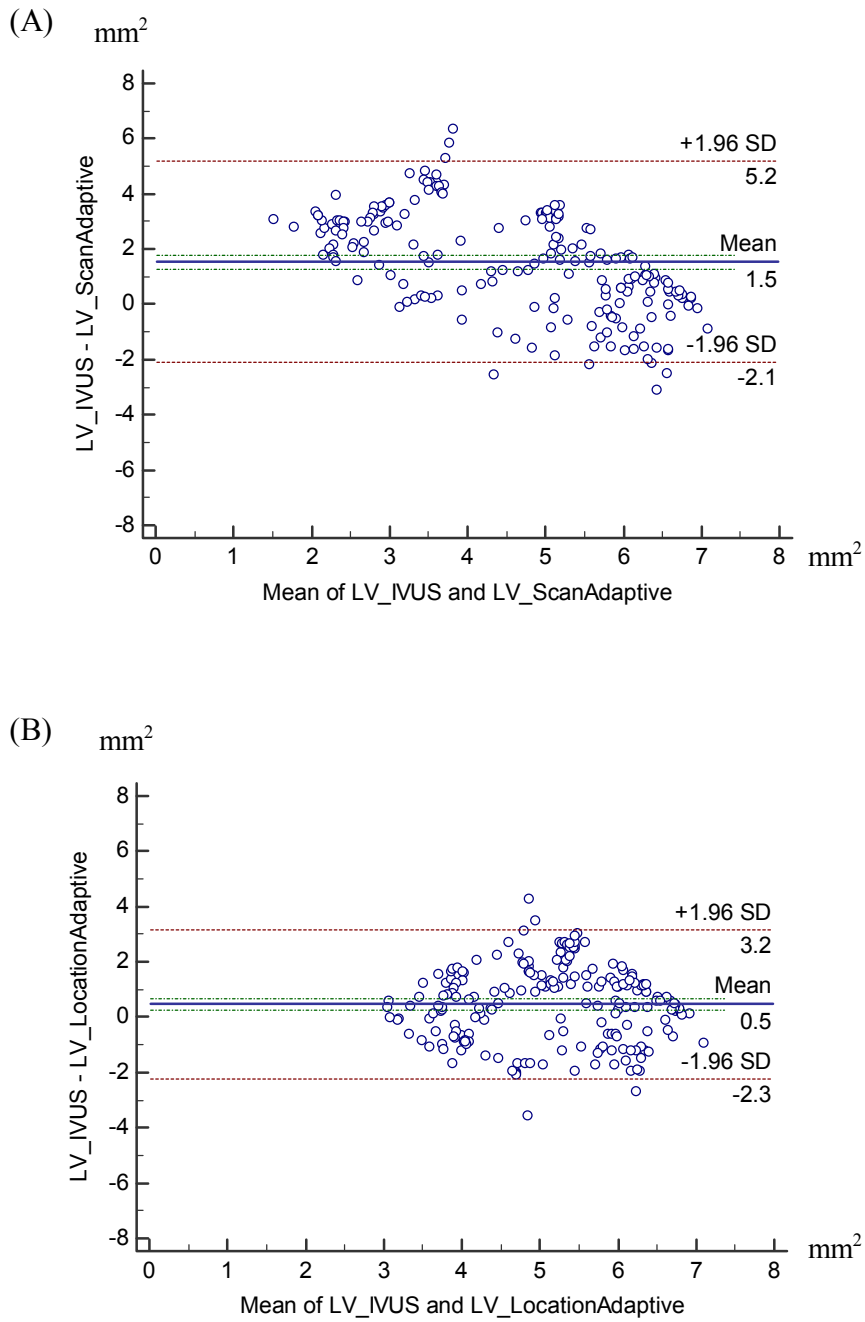

Figure 24. Comparison of lumen area in a subgroup with a lumen area ≥ 7 mm^2. There was no significant difference in the lumen area between location-adaptive and scan-adaptive threshold methods in the subgroup with a large lumen area (n = 112).

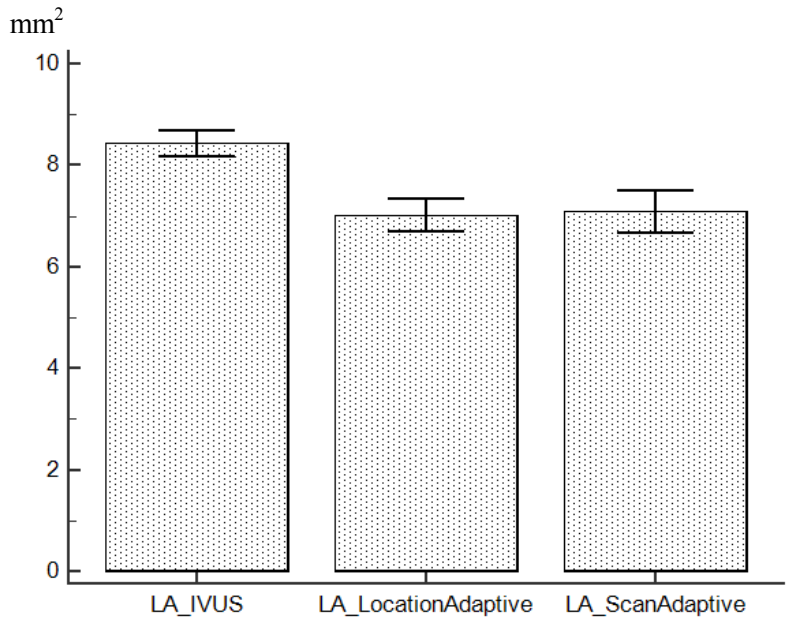

Figure 25. An example of comparison of a scan-adaptive and location-adaptive threshold method for lumen area measurement for a segment with a relatively larger lumen in a 71-year-old female patient. The thickness of each cross section was 0.32 mm, and the total length of the target segment was 15 mm. Reference lumen areas were more than 5 mm^2 for all cross sections. Lumen areas measured by the location-adaptive threshold method were equal to or slightly larger than those calculated using the scan-adaptive threshold method, with an acceptable degree of difference.

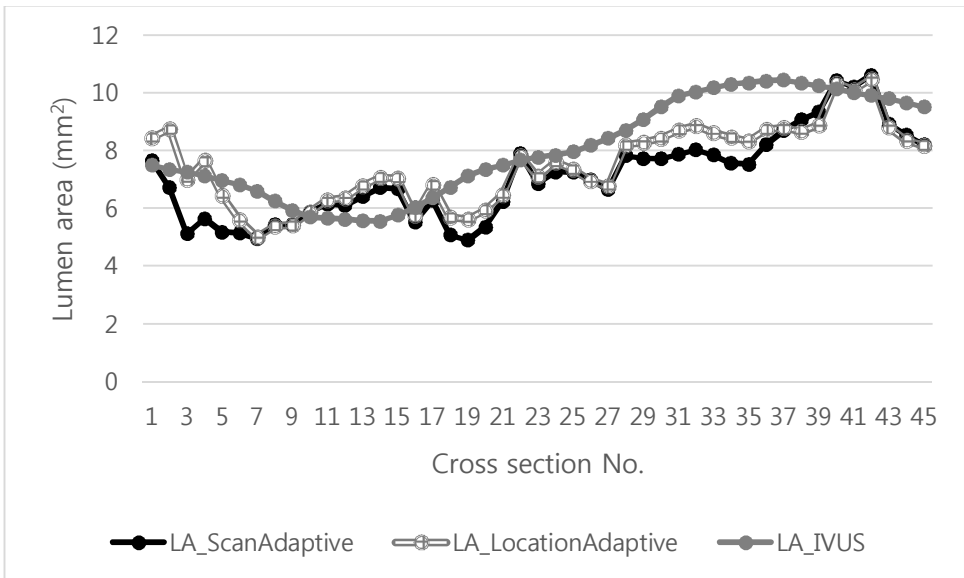

Figure 26. Bland-Altman plot for lumen area in a subgroup with a lumen area ≥ 7 mm².

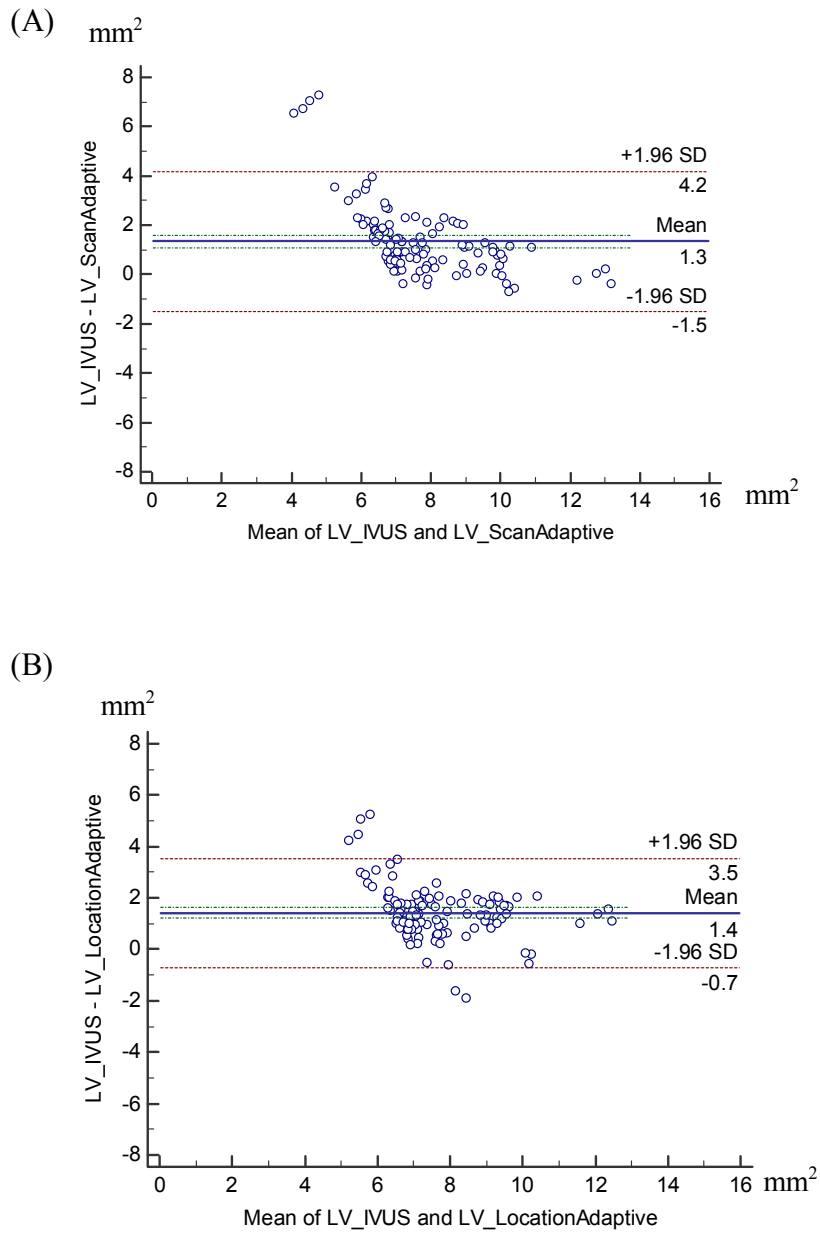

Discussion

The first study in this four-part thesis observed low interplatform reproducibility of the automated plaque volume quantification software as shown by Oberoi et al. in a previous study. In addition, lumen volume measurement was also shown to have low agreement between different automated software programs; therefore, both vessel volume and lumen volume quantifications vary among different automated methods and need to be improved.

Automatic quantification of the vessel volume or vessel area using CCTA is a difficult process because discrimination between epicardial fat and vessel wall is challenging due to the low tissue contrast between them and the limited spatial resolution on CCTA. Several previous studies have shown correlation coefficients of the coronary artery vessel area (as measured by CCTA and IVUS) to be 0.67 to 0.92 when using automated methods (33-36). These can be regarded as a high positive correlation between their measurements based on correlation coefficient values (37). However, this does not signify high accuracy, and there was also significant overestimation (33, 36) or underestimation (34) of the CCTA measurements. Therefore, low reproducibility of the vessel area quantification is not a surprising but rather an expected outcome.

Automated measurement for lumen volume or lumen area of coronary artery seems less challenging compared to the vessel area parameter considering a high contrast between enhanced lumen and vessel wall or plaque along with the long history of technical development in the automatic

analysis for quantitative coronary angiography. However, the reported performance of automated methods for lumen parameters varied and was inadequate. A recent study by Feuchtner et al. showed high correlation coefficients (r = 0.90) between CCTA and IVUS for minimal lumen area and the systemic bias was almost zero (36). However, correlation coefficients in other studies were 0.81-0.84 with a significant underestimation of the CCTA measurement (38,39). However, Voros et al. reported that the minimal lumen area measured by CCTA was significantly overestimated with a correlation coefficient of 0.65 (33). These results indicates that automated methods for lumen segmentation also have to be improved.

Images inherently have blurred edge at the boundary when the real object was imaged with CT and can be presented by a point-spread function of the imaging system (40). The diameter of the imaged object such as vessels was generally characterized by the full width of the profile at 50% of its maximum value (FWHM) calculated from the attenuation profile through the center of the vessel. Therefore, an error can be made if an inadequate threshold was applied in the measurement of lumen diameter. Most commercially available software for the lumen segmentation used threshold methods and the application of a certain value as a threshold for segmentation that ranged from 90 HU to 220 HU (26,41-43). However, each CCTA had a different luminal enhancement degree according to the patient body habitus, scan protocol and parameters; consequently, applying a fixed threshold for all scans might be unsuitable for lumen segmentation and may result in poor interplatform reproducibility as shown in this study. In the same context, Fei et al. demonstrated that the measured stenosis degree could be changed

according to the intraluminal attenuation using a vessel phantom (44). In this study, they simulated coronary artery stenosis containing plaques and filled the vessel lumen with diluted contrast materials that had different attenuation levels. The results showed that 75% simulated stenosis in 3 mm vessel diameter was calculated as 79.3%, 73.7%, and 39.5% in 200 HU along with 300 HU, and 500 HU settings of intraluminal attenuation, respectively. The luminal stenosis was slightly overestimated in 200 HU of the vessel lumen, while it was markedly underestimated in 500 HU. However, this error could be overcome with a different threshold level for a different scan based on enhancement degree. Leber at al. already introduced this kind of concept, setting 65% of the mean intensity within the corresponding lumen as a threshold for lumen segmentation (19) and commercially available software programs such as AUTOPLAQ (45) and QAngio CT (39) do the same.

An important finding of the vessel phantom study was that intraluminal attenuation decreased as lumen size decreased. This finding was sometimes encountered in clinical practice such as SSD or VR image interpretation, but has not been previously investigated in the literature. It partly resulted from a partial volume averaging artifact caused by the relatively low spatial resolution of CT compared to the vessel size. In this study, a pixel resolution of 0.31 mm implies that a vessel with 1 mm diameter is represented by no more than three to four pixels; subsequently, there is a high chance of attenuation averaging with an adjacent low attenuating background because the attenuation value of the vessel center was measured as an average of one center and eight adjacent pixels. However, partial volume averaging might rarely happen because the size of the ROI was small enough

to avoid containing the vessel wall in the larger vessel size. In this condition, one possible explanation would be the inevitable edge blurring of CT image reconstruction by point-spread function.

The phantom study results require further consideration regarding intraluminal attenuation variability especially in segments with stenosis, in addition to variations in setting threshold levels adaptive to the scan in lumen segmentation for use in scan-adaptive threshold method. Therefore, a new concept of a location-adaptive threshold method that reflects a potential intraluminal attenuation variability through a certain segment was devised as described in Part IV Material and Methods.

The phantom study results also generate questions about the emerging concept of the intracoronary transluminal attenuation gradient (TAG). TAG is defined as the linear regression coefficient between luminal attenuation and axial distance from the coronary ostium (46,47). Several studies showed that TAG can predict functionally significant stenosis in coronary arteries (48-51). However, the gradual diminution of intraluminal attenuation from proximal to distal segment might be partly explained by a gradual decrease in lumen size despite the functionally significant stenosis based on the present phantom study result. Further validation studies are therefore warranted for TAG concept because it could be a significant compounding factor in the interpretation of the relationship between TAG and functional stenosis of the coronary artery.

This proof-of-concept study demonstrated that lumen volume measured by the scan-adaptive threshold method was significantly lower than that determined by the reference standard and that this underestimation was

corrected with the application of a location-adaptive threshold method. It is worthwhile that the concept of location-adaptive threshold method could be applied in work related to the segmentation of small vessel lumen that includes coronary arteries such as calculation of luminal stenosis or fractional flow reserve based on CCTA despite the original intent to improve the diagnostic performance of the automated lumen volume quantification as a part of the plaque volume quantification.

The agreement in lumen volume between the location-adaptive threshold method and IVUS was found to be excellent with an ICC value of 0.930. At present, few studies have tried to quantify lumen volume or lumen area using CCTA and compare these with the gold standard derived from IVUS and most of these studies conducted a correlation analysis instead of an agreement analysis which would be a more appropriate analytic method to evaluate the performance of a new measurement system. Therefore, a direct comparison of the performance of the location-adaptive threshold method with previous studies was difficult; however, it can be stated that the location-adaptive threshold method showed better agreement, that the correlation coefficients reported in previous studies ranged from 0.65 to 0.90 (33,36,38,39,41).

In subgroup analysis, the difference in the lumen areas measured by the two different methods was generated in the condition of a smaller lumen size less than 7 mm^2 that corresponded to 3 mm in lumen diameter and not in the larger lumen; subsequently, this result was well in line with the hypothesis. The larger lumen group should indicate a difference in lumen area measurement between scan-adaptive and location-adaptive methods (similar

as in the smaller lumen group) because the phantom study results showed that attenuation differed at more than 3 mm in diameter. However, most of lumen diameter in the larger lumen group was less than 4 mm and CCTA analyzed in this study almost showed an intraluminal peak enhancement around 500 HU. The lumen area calculated from scan- and location-adaptive methods might not be significantly different because the attenuation difference between 3 mm and 4 mm in diameter was small.

In the present study, the mean of the lumen area measured using IVUS was significantly greater than that measured by the location-adaptive method, by approximately 8 % and 17% for the smaller (5.38 mm^2 vs. 4.92 mm^2) and larger (8.43 mm^2 vs. 7.01 mm^2) lumen groups, respectively. This suggests that the lumen area measured by IVUS (the reference standard) and/or CCTA might be inaccurate. IVUS served as the reference standard in this study and has been widely used for the reference standard in coronary atherosclerosis-related studies using CCTA due to its superior spatial resolution compared to CCTA. However, several in vivo studies have shown that IVUS overestimated lumen parameters compared to optical coherence tomography (OCT) (52-55). Some phantom studies have also shown accurate measurements obtained using OCT (55-58). In the phantom study by Kudo et al., the mean of the lumen areas measured using frequency domain OCT was equal to the actual lumen area of the phantom model (7.45 mm^2), and the mean and standard deviations of the lumen area of the phantom measured using IVUS were significantly greater than those measured using OCT (8.03 $\pm$ 0.58 mm^2 vs 7.45 $\pm$ 0.17 mm^2; $P < 0.001$) approximately 8% (55). A possible explanation for significant differences of lumen area between IVUS and

location-adaptive method would be the inaccuracy of the reference standard due to the overestimated value measured by IVUS.

The threshold was set to the half value of the presumed maximum intraluminal attenuation for the application of the threshold for lumen boundary segmentation on CCTA. The attenuation profile of the vessel on cross section shows a three dimensional bell shape and the lowest attenuation value along the vessel boundary might not be zero but variable within a certain range depending on the plaque geometry and composition, whereas the highest attenuation was static. Consequently, the half maximum value which served as the threshold for segmentation might be also variable along the vessel boundary and it may not be a single value on a cross section set to a half of the maximum intraluminal attenuation value in the present study. This potential error can be cause for a lower agreement in the lumen area (ICC, 0.668) measured by IVUS and the location-adaptive threshold method than in the lumen volume (ICC, 0.945). Follow up studies using an additional adaptive threshold along each vessel boundary are warranted for more accurate and precise measurements.

Some limitations should be considered. First, the sample size was relatively small. However, subgroup analysis per cross-section was performed with a sufficient number that provided more detailed information. Second, there is potential to mismatch the target segment between IVUS and CCTA; however, the degree of mismatch was believe only to be a trace since it was double-checked with references of text and image. There was some mismatch because a certain value of z-spacing in CCTA hinder the exact synchronization of the cross section with IVUS under the condition of

matching cross sections which cannot be calculated by multiplying the 1/60 mm, a fixed frame thickness of IVUS. However, this is not a factor to overcome because of the inherent nature of imaging modalities. Efforts were made to minimize the degree of mismatch of cross section instead. Finally, the proposed location-adaptive threshold method was not compared with commercially available software programs that introduced the concept of a scan-adaptive threshold method.

In conclusion, based on the results of the phantom study, which indicate that intraluminal attenuation decreases with diminution of vessel diameters, a novel concept for lumen segmentation, referred to herein as the location-adaptive threshold method, is proposed. Using this method, a lower attenuation value is applied in stenotic locations within a target segment for edge detection between the lumen and vessel wall. The location-adaptive threshold method was shown to more accurate than the scan-adaptive threshold method for lumen segmentation.

References

1. Nissen SE, Nicholls SJ, Sipahi I, Libby P, Raichlen JS, Ballantyne CM, et al. Effect of very high-intensity statin therapy on regression of coronary atherosclerosis - The ASTEROID trial. JAMA. 2006;295(13):1556-65.
2. Gao WQ, Feng QZ, Li YF, Li YX, Huang Y, Chen YM, et al. Systematic study of the effects of lowering low-density lipoprotein-cholesterol on regression of coronary atherosclerotic plaques using intravascular ultrasound. BMC Cardiovasc Disord. 2014;14:60.
3. Puri R, Nissen SE, Shao M, Ballantyne CM, Barter PJ, Chapman MJ, et al. Coronary atheroma volume and cardiovascular events during maximally intensive statin therapy. Eur Heart J. 2013;34(41):3182-90.
4. Shan P, Mintz GS, McPherson JA, De Bruyne B, Farhat NZ, Marso SP, et al. Usefulness of coronary atheroma burden to predict cardiovascular events in patients presenting with acute coronary syndromes (from the PROSPECT Study). Am J Cardiol. 2015;116(11):1672-7.
5. Nicholls SJ, Hsu A, Wolski K, Hu B, Bayturan O, Lavoie A, et al. Intravascular ultrasound-derived measures of coronary atherosclerotic plaque burden and clinical outcome. J Am Coll Cardiol. 2010;55(21):2399-407.
6. Puri R, Worthley MI, Nicholls SJ. Intravascular imaging of vulnerable coronary plaque: current and future concepts. Nat Rev Cardiol. 2011;8(3):131-9.
7. Mintz GS. Clinical utility of intravascular imaging and physiology in coronary artery disease. J Am Coll Cardiol. 2014;64(2):207-22.
8. Montalescot G, Sechtem U, Achenbach S, Andreotti F, Arden C, Budaj A, et al. 2013 ESC guidelines on the management of stable coronary artery disease: The task force on the management of stable coronary artery disease of the European Society of Cardiology. Eur Heart J. 2013;34(38):2949-3003.
9. Guo SL, Guo YM, Zhai YN, Ma B, Wang P, Yang KH. Diagnostic accuracy of first generation dual-source computed tomography in the assessment of coronary artery disease: A meta-analysis from 24 studies. Int J Cardiovasc Imaging. 2011;27(6):755-71.

10. Baumann S, Renker M, Meinel FG, Wichmann JL, Fuller SR, Bayer RR, 2nd, et al. Computed tomography imaging of coronary artery plaque: characterization and prognosis. Radiol Clin North Am. 2015;53(2):307-15.
11. Schroeder S, Kopp AF, Baumbach A, Meisner C, Kuettner A, Georg C, et al. Noninvasive detection and evaluation of atherosclerotic coronary plaques with multislice computed tomography. J Am Coll Cardiol. 2001;37(5):1430-5.
12. Motoyama S, Kondo T, Anno H, Sugiura A, Ito Y, Mori K, et al. Atherosclerotic plaque characterization by 0.5-mm-slice multislice computed tomographic imaging. Circ J. 2007;71(3):363-6.
13. Achenbach S, Moselewski F, Ropers D, Ferencik M, Hoffmann U, MacNeill B, et al. Detection of calcified and noncalcified coronary atherosclerotic plaque by contrast-enhanced, submillimeter multidetector spiral computed tomography - A segment-based comparison with intravascular ultrasound. Circulation. 2004;109(1):14-7.
14. Moselewski F, Ropers D, Pohle K, Hoffmann U, Ferencik M, Chan RC, et al. Comparison of measurement of cross-sectional coronary atherosclerotic plaque and vessel areas by 16-slice multidetector computed tomography versus intravascular ultrasound. Am J Cardiol. 2004;94(10):1294-7.
15. Petranovic M, Soni A, Bezzera H, Loureiro R, Sarwar A, Raffel C, et al. Assessment of nonstenotic coronary lesions by 64-slice multidetector computed tomography in comparison to intravascular ultrasound: evaluation of nonculprit coronary lesions. J Cardiovasc Comput Tomogr. 2009;3(1):24-31.
16. Schepis T, Achenbach S, Weyand M, Raum P, Marwan M, Pflederer T, et al. Comparison of dual source computed tomography versus intravascular ultrasound for evaluation of coronary arteries at least one year after cardiac transplantation. Am J Cardiol. 2009;104(10):1351-6.
17. Papadopoulou SL, Neefjes LA, Schaap M, Li HL, Capuano E, van der Giessen AG, et al. Detection and quantification of coronary atherosclerotic plaque by 64-slice multidetector CT: A systematic head-to-head comparison with intravascular ultrasound. Atherosclerosis. 2011;219(1):163-70.
18. Dey D, Schuhbaeck A, Min JK, Berman DS, Achenbach S. Non-invasive measurement

of coronary plaque from coronary CT angiography and its clinical implications. Expert Rev Cardiovasc Ther. 2013;11(8):1067-77.

19. Leber AW, Becker A, Knez A, von Ziegler F, Sirol M, Nikolaou K, et al. Accuracy of 64-slice computed tomography to classify and quantify plaque volumes in the proximal coronary system—A comparative study using intravascular ultrasound. J Am Coll Cardiol. 2006;47(3):672-7.
20. Pflederer T, Schmid M, Ropers D, Ropers U, Komatsu S, Daniel WG, et al. Interobserver variability of 64-slice computed tomography for the quantification of non-calcified coronary atherosclerotic plaque. Rofo. 2007;179(9):953-7.
21. Schuhbaeck A, Dey D, Otaki Y, Slomka P, Kral BG, Achenbach S, et al. Interscan reproducibility of quantitative coronary plaque volume and composition from CT coronary angiography using an automated method. Eur Radiol. 2014;24(9):2300-8.
22. Brodoefel H, Burgstahler C, Heuschmid M, Reimann A, Khosa F, Kopp A, et al. Accuracy of dual-source CT in the characterisation of non-calcified plaque: use of a colour-coded analysis compared with virtual histology intravascular ultrasound. Br J Radiol. 2009;82(982):805-12.
23. Rinehart S, Vazquez G, Qian Z, Murrieta L, Christian K, Voros S. Quantitative measurements of coronary arterial stenosis, plaque geometry, and composition are highly reproducible with a standardized coronary arterial computed tomographic approach in high-quality CT datasets. J Cardiovasc Comput Tomogr. 2011;5(1):35-43.
24. Papadopoulou SL, Garcia-Garcia HM, Rossi A, Girasis C, Dharampal AS, Kitslaar PH, et al. Reproducibility of computed tomography angiography data analysis using semiautomated plaque quantification software: implications for the design of longitudinal studies. Int J Cardiovasc Imaging. 2013;29(5):1095-104.
25. Lee MS, Chun EJ, Kim KJ, Kim JA, Vembar M, Choi SI. Reproducibility in the assessment of noncalcified coronary plaque with 256-slice multi-detector CT and automated plaque analysis software. Int J Cardiovasc Imaging. 2010;26(Suppl 2):237-44.
26. Oberoi S, Meinel FG, Schoepf UJ, Nance JW, De Cecco CN, Gebregziabher M, et al. Reproducibility of noncalcified coronary artery plaque burden quantification from

coronary CT angiography across different image analysis platforms. AJR Am J Roentgenol. 2014;202(1):W43-9.

27. Abbara S, Arbab-Zadeh A, Callister TQ, Desai MY, Mamuya W, Thomson L, et al. SCCT guidelines for performance of coronary computed tomographic angiography: A report of the Society of Cardiovascular Computed Tomography Guidelines Committee. J Cardiovasc Comput Tomogr. 2009;3(3):190-204.
28. Gonzalez RC, Woods RE. Morphologic imaging processing and Image segmentation. In: Digital Imaging Processing. 3rd ed. New Jersey: Pearson Prentice Hall, 2008; 627-794.
29. Kruk M, Wardziak L, Mintz GS, Achenbach S, Pregowski J, Ruzyllo W, et al. Accuracy of coronary computed tomography angiography vs intravascular ultrasound for evaluation of vessel area. J Cardiovasc Comput Tomogr. 2014;8(2):141-8.
30. Brodoefel H, Burgstahler C, Sabir A, Yam C-S, Khosa F, Claussen CD, et al. Coronary plaque quantification by voxel analysis: Dual-source MDCT angiography versus intravascular sonography. AJR Am J Roentgenol. 2009;192(3):W84-W9.
31. Clouse ME, Sabir A, Yam C-S, Yoshimura N, Lin S, Welty F, et al. Measuring noncalcified coronary atherosclerotic plaque using voxel analysis with MDCT angiography: A pilot clinical study. AJR Am J Roentgenol. 2008;190(6):1553-60.
32. Bland JM, Altman DG. Measuring agreement in method comparison studies. Stat Methods Med Res. 1999;8(2):135-60.
33. Voros S, Rinehart S, Qian Z, Vazquez G, Anderson H, Murrieta L, et al. Prospective validation of standardized, 3-dimensional, quantitative coronary computed tomographic plaque measurements using radiofrequency backscatter intravascular ultrasound as reference standard in intermediate coronary arterial lesions: results from the ATLANTA (assessment of tissue characteristics, lesion morphology, and hemodynamics by angiography with fractional flow reserve, intravascular ultrasound and virtual histology, and noninvasive computed tomography in atherosclerotic plaques) I study. JACC Cardiovasc Interv. 2011;4(2):198-208.
34. Bruining N, Roelandt JRTC, Palumbo A, La Grutta L, Cademartiri F, de Feijter PJ, et al. Reproducible coronary plaque quantification by multislice computed tomography.

Catheter Cardiovasc Interv. 2007;69(6):857-65.

35. Brodoefel H, Reimann A, Heuschmid M, Tsiflikas I, Kopp AF, Schroeder S, et al. Characterization of coronary atherosclerosis by dual-source computed tomography and HU-based color mapping: a pilot study. Eur Radiol. 2008;18(11):2466-74.
36. Feuchtner G, Loureiro R, Bezerra H, Rocha-Filho JA, Sarwar A, Pflederer T, et al. Quantification of coronary stenosis by dual source computed tomography in patients: A comparative study with intravascular ultrasound and invasive angiography. Eur J Radiol. 2012;81(1):83-8.
37. Mukaka MM. Statistics corner: A guide to appropriate use of correlation coefficient in medical research. Malawi Med J. 2012;24(3):69-71.
38. Sun J, Zhang Z, Lu B, Yu W, Yang Y, Zhou Y, et al. Identification and quantification of coronary atherosclerotic plaques: A comparison of 64-MDCT and intravascular ultrasound. AJR Am J Roentgenol. 2008;190(3):748-54.
39. Boogers MJ, Broersen A, van Velzen JE, de Graaf FR, El-Naggar HM, Kitslaar PH, et al. Automated quantification of coronary plaque with computed tomography: Comparison with intravascular ultrasound using a dedicated registration algorithm for fusion-based quantification. Eur Heart J. 2012;33(8):1007-16.
40. Kalender WA. Image quality. In: Computed Tomography. 3rd ed. Erlangen: Publicis, 2011; 111-72.
41. Akutagawa O, Kijima Y, Kume K, Sakai T, Okura A, Ide K, et al. Feasibility and limitation of coronary plaque volumetry by contrast-enhanced 64-row multi-detector computed tomography. Int J Cardiol. 2011;150(1):118-20.
42. Blackmon KN, Streck J, Thilo C, Bastarrika G, Costello P, Schoepf UJ. Reproducibility of automated noncalcified coronary artery plaque burden assessment at coronary CT angiography. J Thorac Imaging. 2009;24(2):96-102.
43. Kim YJ, Jin GY, Kim EY, Han YM, Chae JK, Lee SR, et al. Quantification of coronary artery plaque using 64-slice dual-source CT: comparison of semi-automatic and automatic computer-aided analysis based on intravascular ultrasonography as the gold standard. Int J Cardiovasc Imaging. 2013;29(Suppl 2):93-100.
44. Fei X, Du X, Yang Q, Shen Y, Li P, Liao J, et al. 64-MDCT coronary angiography:

phantom study of effects of vascular attenuation on detection of coronary stenosis. AJR Am J Roentgenol. 2008;191(1):43-9.

45. Dey D, Schepis T, Marwan M, Slomka PJ, Berman DS, Achenbach S. Automated three-dimensional quantification of noncalcified coronary plaque from coronary CT angiography: Comparison with intravascular US. Radiology. 2010;257(2):516-22.
46. Steigner ML, Mitsouras D, Whitmore AG, Otero HJ, Wang C, Buckley O, et al. Iodinated contrast opacification gradients in normal coronary arteries imaged with prospectively ECG-gated single heart beat 320-detector row computed tomography. Circ Cardiovasc Imaging. 2010;3(2):179-86.
47. Ko BS, Wong DT, Norgaard BL, Leong DP, Cameron JD, Gaur S, et al. Diagnostic performance of transluminal attenuation gradient and noninvasive fractional flow reserve derived from 320-detector row CT angiography to diagnose hemodynamically significant coronary stenosis: An NXT substudy. Radiology. 2016;279(1):75-83.
48. Choi JH, Min JK, Labounty TM, Lin FY, Mendoza DD, Shin DH, et al. Intracoronary transluminal attenuation gradient in coronary CT angiography for determining coronary artery stenosis. JACC Cardiovasc Imaging. 2011;4(11):1149-57.
49. Chow BJ, Kass M, Gagne O, Chen L, Yam Y, Dick A, et al. Can differences in corrected coronary opacification measured with computed tomography predict resting coronary artery flow? J Am Coll Cardiol. 2011;57(11):1280-8.
50. Wong DT, Ko BS, Cameron JD, Nerlekar N, Leung MC, Malaiapan Y, et al. Transluminal attenuation gradient in coronary computed tomography angiography is a novel noninvasive approach to the identification of functionally significant coronary artery stenosis: a comparison with fractional flow reserve. J Am Coll Cardiol. 2013;61(12):1271-9.
51. Choi JH, Kim EK, Kim SM, Song YB, Hahn JY, Choi SH, et al. Noninvasive evaluation of coronary collateral arterial flow by coronary computed tomographic angiography. Circ Cardiovasc Imaging. 2014;7(3):482-90.
52. Yamaguchi T, Terashima M, Akasaka T, Hayashi T, Mizuno K, Muramatsu T, et al. Safety and feasibility of an intravascular optical coherence tomography image wire system in the clinical setting. Am J Cardiol. 2008;101(5):562-7.

53. Capodanno D, Prati F, Pawlowsky T, Cera M, La Manna A, Albertucci M, et al. Comparison of optical coherence tomography and intravascular ultrasound for the assessment of in-stent tissue coverage after stent implantation. EuroIntervention. 2009;5(5):538-43.

54. Okamura T, Onuma Y, Garcia-Garcia HM, van Geuns RJ, Wykrzykowska JJ, Schultz C, et al. First-in-man evaluation of intravascular optical frequency domain imaging (OFDI) of Terumo: a comparison with intravascular ultrasound and quantitative coronary angiography. EuroIntervention. 2011;6(9):1037-45.

55. Kubo T, Akasaka T, Shite J, Suzuki T, Uemura S, Yu B, et al. OCT compared with IVUS in a coronary lesion assessment: the OPUS-CLASS study. JACC Cardiovasc Imaging. 2013;6(10):1095-104.

56. Tahara S, Bezerra HG, Baibars M, Kyono H, Wang W, Pokras S, et al. In vitro validation of new Fourier-domain optical coherence tomography. EuroIntervention. 2011;6(7):875-82.

57. Sawada T, Shite J, Negi N, Shinke T, Tanino Y, Ogasawara D, et al. Factors that influence measurements and accurate evaluation of stent apposition by optical coherence tomography. Assessment using a phantom model. Circ J. 2009;73(10):1841-7.

58. Tsuchida K, van der Giessen WJ, Patterson M, Tanimoto S, Garcia-Garcia HM, Regar E, et al. In vivo validation of a novel three-dimensional quantitative coronary angiography system (CardiOp-B): comparison with a conventional two-dimensional system (CAAS II) and with special reference to optical coherence tomography. 2007;3(1):100-8

초록

배경: 전산화단층촬영 영상 기반 관상동맥경화반 용적 자동 측정은 기존의 침습적인 혈관내초음파나 시간 투입형인 수동측정법을 대신하여 시도되어 왔다. 자동측정법은 유망한 결과들을 보여주고 있지만, 방법 간 재현성은 그렇게 좋지 않았다.

목적: 이 연구의 목적은 1) 경화반 자동측정법 간 재현성에 영향을 미치는 변수를 탐색하고, 2) 모형을 이용하여 혈관 내경에 따라 혈관 내 감쇠값이 다름을 증명하며, 3) 혈관 외부 경계에 대한 자동 분할 알고리즘을 개발하여, 4) 혈관 내부 경계 분할에 대한 새로운 개념을 제안하고 이를 입증하는 것이다.

방법: 네 부분으로 이루어진 연구 중 첫 번째로, 세 개의 상용화된 프로그램을 이용하여 총 17개의 관상동맥 표적 분절에 대해 총 경화반 부피 및 내강 부피를 자동적으로 측정하여 각 프로그램 간의 일치도를 평가하였으며, 참조 표준으로 삼은 혈관내초음파와도 비교하였다. 두 번째로, 각각 다른 내경을 가지는 다양한 혈관 모형에 동일한 농도의 조영제에 채워 전산화단층촬영을 시행하고 각 내강의 감쇠값을 측정하였다. 혈관 외부 경계를 자동 분할하는 프로그램은 1) 영역 성장법을 이용한 대강의 관 모양 형성, 2) 가장 낮은 경로 비용을 보이는 초기 중심선 추출, 3) 초기 중심선을 중심으로 곡면 재구성 및 직각을 교차되는 평면 형성, 4) 누출 보간, 롤링 볼을 이용한 곡선 근사 그리고 볼록 껍질 알고리즘을 이용한 외부 경계 결정, 5) 무게 중심을 이용한 최종 중심선 결정, 순으로 개발되었다. 내강과 혈관 벽의 경계를 결정하는데 있어서, 한 개의 특정 문턱값을 표적 분절 전체에 적용하는

스캔 적응 분할 방법에서 진일보한, 혈관 내의 다양한 협착 위치에서 각각에 적절한 낮은 감쇠 값으로 이루어진 별도의 문턱값을 적용하는 위치 적응 분할 방법이라는 새로운 개념을 고안하였다. 이 새로운 개념을 입증하기 위해 15명 환자의 전산화단층촬영에서 얻은 22개의 표적 분절의 각각의 단면에 스캔 적응 분할 방법과 위치 적응 분할 방법을 이용하여 내강 부피와 총 경화반 부피를 계산하고, 이를 참조 표준인 혈관내초음파에서 얻은 값과 비교하였다. 또한, 비석회성 경화반으로 이루어진 표적 분절들의 각각의 단면에서 내강 면적을 계산하고, 내경에 따라 하위집단 분석을 시행하였다.

결과: 상용화된 프로그램으로 자동측정한 총 경화반 부피와 내강 부피의 급내 상관 계수는 각각 0.309에서 0.482, 그리고 0.759였다. 모형실험에서는 각 혈관이 같은 농도의 조영제로 채워져 있음에도 혈관 내강의 감쇠값이 혈관 내경이 감소함에 따라 작아졌다. 혈관 외부 경계를 분할하는 새로 개발한 프로그램은 혈관 부피 측정에서 혈관 내 초음파와 우수한 일치도를 보였다 (급내 상관 계수, 0.919). 새로운 개념을 입증하는 연구에서 혈관내초음파와 위치 적응 분할 방법을 이용하여 측정한 내강 부피와 (평균 ± 표준오차, 93.0 ± 11.2 mm^3 대 93.7 ± 10.0 mm^3) 총 경화반 부피 (114.4 ± 11.4 mm^3대 125.7 ± 15.5 mm^3)의 평균값은 유의하게 다르지 않았다 (P=0.999). 스캔 적응 분할 방법을 이용한 경우, 내강 부피는 (78.4 ± 10.2 mm^3) 유의하게 과소평가되었고, 총 경화반 부피는 (141.1 ± 16.4 mm^3) 유의하게 과대평가되었다 (P<0.05). 내강 부피에 대한 참조 표준과의 일치도는 위치 적응 분할 방법이 (급내 상관 계수, 0.930) 스캔 적응 분할 방법보다 (급내 상관 계수, 0.872) 좋았다. 하위집단 분석에서 스캔

적응 분할 방법과 위치 적응 분할 방법 사이의 내강 면적 평균값의 차이는 내강이 작은 집단에서는 유의하였지만 (3.85 mm^2 대 4.92 mm^2, P<0.001), 내강이 큰 집단에서는 유의하지 않았다 (7.09 mm^2 대 7.01 mm^2, P=0.336).

결론: 내경감소에 따라 내강 감쇠값이 감소한다는 모형 실험 결과에 근거하여, 혈관 내강 분할에 관한 독창적인 개념인 위치 적응 분할 방법이 제안되었고, 이 방법은 스캔 적응 분할 방법보다 정확하였다.

주요어: 위치 적응 분할 방법, 스캔 적응 분할 방법, 경화반, 관상동맥 전산화단층촬영, 경화반 자동 정량화, 관상동맥, 반치전폭, 혈관내초음파

학번: 2008-31012